Title

Mechanosensitive mTORC2 independently coordinates leading and trailing edge polarity programs during neutrophil migration

Journal

Molecular Biology of the Cell, 34(5)

ISSN

1059-1524

Authors

Saha, Suvrajit
Town, Jason P
Weiner, Orion D

Publication Date

2023-05-01

DOI

10.1091/mbc.e22-05-0191

Mechanosensitive mTORC2 independently coordinates leading and trailing edge polarity programs during neutrophil migration

Suvrajit Saha, Jason P. Town, and Orion D. Weiner*
Cardiovascular Research Institute and Department of Biochemistry and Biophysics, University of California, San Francisco, CA 94158

ABSTRACT **By acting both upstream of and downstream from biochemical organizers of the cytoskeleton, physical forces function as central integrators of cell shape and movement. Here we use a combination of genetic, pharmacological, and optogenetic perturbations to probe the role of the conserved mechanosensitive mTOR complex 2 (mTORC2) programs in neutrophil polarity and motility. We find that the tension-based inhibition of leading-edge signals (Rac, F-actin) that underlies protrusion competition is gated by the kinase-independent role of the complex, whereas the regulation of RhoA and myosin II–based contractility at the trailing edge depend on mTORC2 kinase activity. mTORC2 is essential for spatial and temporal coordination of the front and back polarity programs for persistent migration under confinement. This mechanosensory pathway integrates multiple upstream signals, and we find that membrane stretch synergizes with biochemical co-input phosphatidylinositol (3,4,5)-trisphosphate to robustly amplify mTORC2 activation. Our results suggest that different signaling arms of mTORC2 regulate spatially and molecularly divergent cytoskeletal programs for efficient coordination of neutrophil shape and movement.**

Monitoring Editor
Anna Huttenlocher
University of Wisconsin, Madison

Received: May 31, 2022
Revised: Jan 24, 2023
Accepted: Feb 23, 2023

INTRODUCTION

Directed cell migration underlies a wide range of physiological processes ranging from developmental morphogenesis to immune cell responses (SenGupta *et al.*, 2021). Single cells move by extending a leading front that protrudes and a trailing rear that contracts and follows the front. These programs exhibit not only spatial compartmentalization of distinct intracellular signals to either the front or back of the cell (polarization) but also temporal coordination between these domains (Xu *et al.*, 2003). Neutrophils are a type of innate immune cell that rely on properly oriented cell polarity to migrate to sites of injury where they hunt and kill invading pathogens (Lämmermann *et al.*, 2013). At the cell front, activation of small GTPase Rac helps sets the permissive zone for WAVE-regulatory complex–dependent actin polymerization in protrusions (Weiner *et al.*, 2007; Koronakis *et al.*, 2011). At the back, the GTPase RhoA stimulates myosin-based contractility (Wong *et al.*, 2006; Hind *et al.*, 2016; Tsai *et al.*, 2019). These signaling domains are sustained by short-range positive feedback loops within the modules and are spatially separated by mutual antagonism between them (Xu *et al.*, 2003; Ku *et al.*, 2012). Coordination within and between the modules is critical for polarity maintenance during persistent migration (Tsai *et al.*, 2019), but how this coordination is achieved is not fully understood.

When cells protrude or contract, they alter the mechanical properties of the cell surface. While mechanics was initially seen as a downstream output of cytoskeletal dynamics, emerging evidence suggests that mechanics feeds back to regulate the upstream leading and trailing edge biochemical signals (Diz-Muñoz *et al.*, 2013;

This article was published online ahead of print in MBoC in Press (http://www.molbiolcell.org/cgi/doi/10.1091/mbc.E22-05-0191) on March 1, 2023.

The authors declare no competing financial interests.

Author contributions: S.S. and O.D.W. conceptualized the study; S.S. and J.P.T. performed the investigation and data curation; S.S. and J.P.T. performed the formal analysis; S.S. and J.P.T. developed the reagents and methodology; S.S., J.P.T., and O.D.W. contributed to funding acquisition; J.P.T. provided the software; S.S. and J.P.T. provided visualization and figures; S.S. wrote and revised the original draft with edits and inputs from O.D.W. and J.P.T.

*Address correspondence to: Orion D. Weiner (orion.weiner@ucsf.edu).

Abbreviations used: dHL-60, differentiated HL-60 cell; F-actin, filamentous actin; fMLP, N-formylmethionine-leucyl-phenylalanine; mTOR, mechanistic target of rapamycin; mTORC2, mTOR complex 2; PIP_3, phosphatidylinositol (3,4,5)-trisphosphate; PI3K, phosphoinositide 3-kinase; pMLC, phosphorylated myosin regulatory light chain; pPAK, phosphorylated p21-activated kinase; Rac, Ras-related C3 botulinum toxin substrate; shRNA, small hairpin RNA.

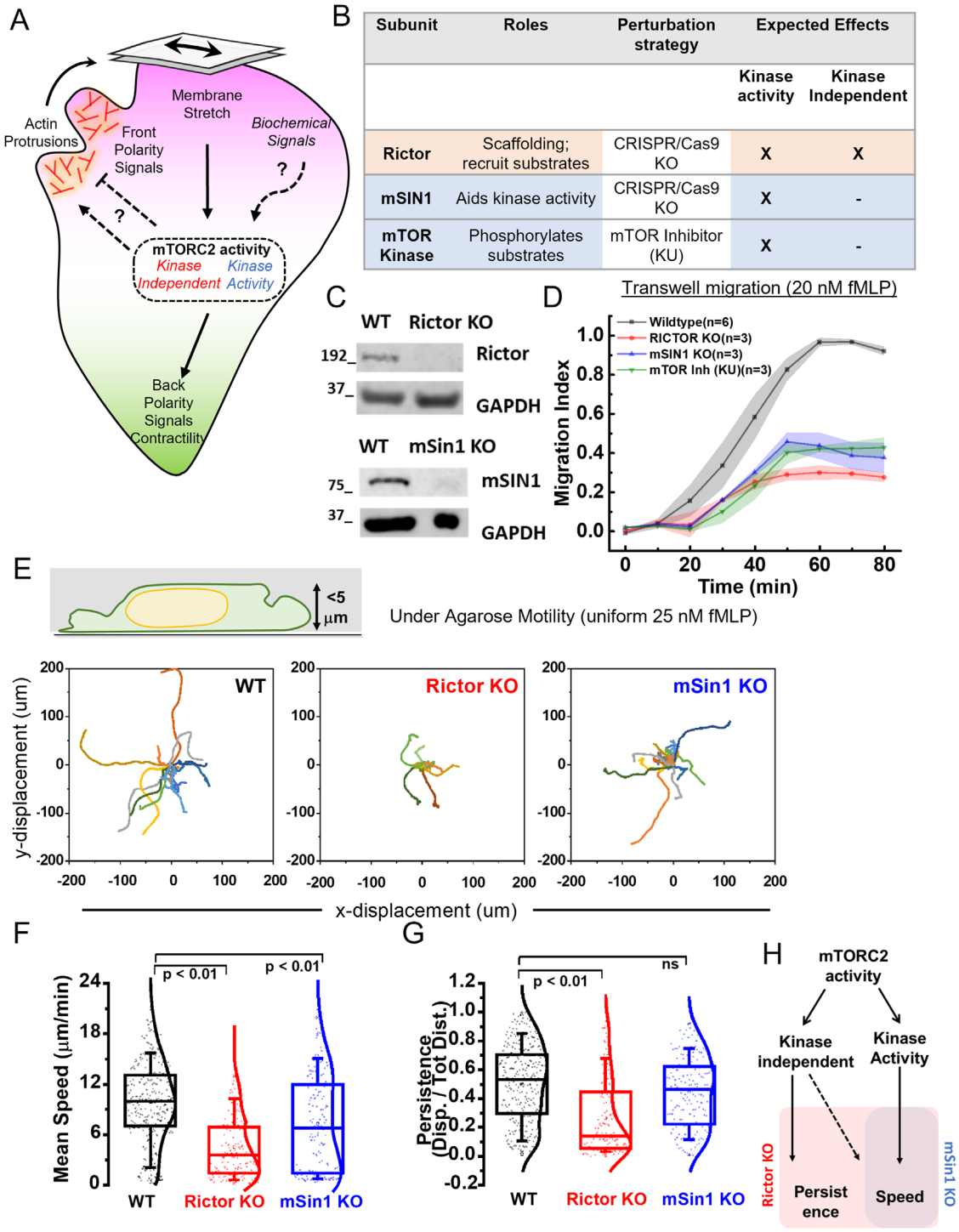

FIGURE 1: Rictor/mTORC2 is a regulator of neutrophil motility. (A) mTORC2 connects membrane stretch to regulation of front (magenta) and back (green) polarity programs, but how mTORC2 is activated (purely mechanical or requires biochemical co-inputs) and what aspect of mTORC2 activation (kinase-dependent vs. independent roles) regulates these polarity signals is not understood. (B) To dissect the roles of kinase-dependent and kinase-independent roles of mTORC2, we generated individual CRISPR-Cas9 knockout lines of key components of the complex: Rictor (which scaffolds and aids structural integrity of the complex) or mSin1 (which primarily aids kinase activity). Additionally, we use mTOR kinase inhibitors (here KU-0063794; KU) to phenocopy mSin1 KO defects. (C) Representative immunoblots of wild-type (WT) HL-60 cells and gene-edited Rictor KO (top) and mSin1 KO (bottom) clonal HL-60 line to validate the loss of Rictor or mSin1 protein expression. GAPDH was used as a loading control. (D) Perturbation of mTORC2 activities in Rictor KO ($n = 3$; red), mSin1 KO ($n = 3$; blue), and via mTOR kinase inhibitor (KU; $n = 3$; green) all led to defective transwell migration toward chemoattractant 20 nM fMLP in comparison to WT cells ($n = 6$; black). Mean ± SEM is plotted; n indicates independent replicates. (E) Schematic shows neutrophil-like dHL60 cell moving under an agarose (2%) overlay with uniform chemoattractant (25 nM fMLP). Randomly chosen representative tracks (15 each) of wild-type

Mueller *et al.*, 2017; Saha *et al.*, 2018; Hetmanski *et al.*, 2019). In neutrophils, membrane tension acts as a long-range inhibitor of actin nucleation and polymerization to constrain the size and number of cell protrusions (Houk *et al.*, 2012). Increases in membrane tension triggers a mechanosensitive signaling cascade to regulate actin dynamics in neutrophils. Actin-based polymerization in protrusions stimulates mechanistic target of rapamycin complex 2 (mTORC2) through the activation of phospholipase D2. By connecting increases in protrusion to decreases in actin nucleation, mTORC2 is a central component of the negative-feedback–based homeostat on membrane tension (Diz-Muñoz *et al.*, 2016).

mTOR kinase is an ancient and evolutionarily conserved regulator of cell growth, proliferation, and survival (Saxton and Sabatini, 2017). mTOR forms two distinct multisubunit complexes in mammalian cells mTOR complex 1 (mTORC1) and mTOR complex 2 (mTORC2). mTORC2 is formed from the association of core mTOR subunits with Rictor and mSin1. Rictor scaffolds the complex and is indispensable for the stability of the complex, whereas mSin1 aids the kinase activity of the complex (Jacinto *et al.*, 2004; Sarbassov *et al.*, 2004; Frias *et al.*, 2006). TORC2 activity is thought to broadly localize to plasma membrane (Ebner *et al.*, 2017b; Riggi *et al.*, 2020), where it relays growth factor signals by phosphorylating its downstream effectors Akt, PKC, and SGK1 and other targets to regulate a wide range of cellular processes including cytoskeletal organization and cell migration (Saxton and Sabatini, 2017).

mTORC2 plays a homeostatic role in response to membrane stretch in a wide variety of cell types, ranging from yeast (Berchtold *et al.*, 2012; Riggi *et al.*, 2018) to immune cells (Diz-Muñoz *et al.*, 2016) to *Dictyostelium* (Kamimura *et al.*, 2008). In *Saccharomyces cerevisiae*, plasma membrane (PM) stretch activates TORC2 to stimulate sphingolipid biosynthesis, sterol recycling, and bilayer asymmetry as homeostatic mechanisms to reset membrane tension and restore membrane trafficking (Riggi *et al.*, 2020). In neutrophils, where membrane tension increases arise from protrusive forces of F-actin, mTORC2-based inhibition of actin polymerization serves a mechanism to maintain the tension set point as well as restrict polarity signals (Diz-Muñoz *et al.*, 2016). A conserved role of mTORC2 also involves gating chemoattractant signaling to cyclic-AMP production to regulate myosin contractility and drive tail retraction in neutrophils (Liu *et al.*, 2010, 2014). Perturbation of mTORC2 component Rictor led to impaired chemotaxis in neutrophils, fibroblasts, and *Dictyostelium* consistent with its role in regulating actin cytoskeleton (Lee *et al.*, 2005; Liu *et al.*, 2010; Agarwal *et al.*, 2013; He *et al.*, 2013). These wide arrays of cytoskeletal defects are thought to rise from both positive (He *et al.*, 2013) and negative inputs (Diz-Muñoz *et al.*, 2016; Huang *et al.*, 2017) to front and back polarity programs and have been difficult to decouple.

Here, we investigate the logic of Rictor/mTORC2-based regulation of front and back polarity programs (Figure 1A). The kinase-independent roles of mTORC2 restricts actin polymerization at the cell front, whereas its kinase activity is essential for myosin contractility at the cell rear. While front/back regulation is normally highly coordinated during movement, cells lose their coordination in the absence of mTORC2. These defects are particularly profound when neutrophils explore and move in confined environments. Furthermore, membrane stretch synergizes with biochemical co-input of PIP_3 to robustly amplify mTORC2 signaling activity. Our work reveals a role for mTORC2 in coordinating front and back polarity through different effector arms of this highly conserved mechanosensor.

RESULTS

Rictor/mTORC2 is a regulator of neutrophil ameboid motility

How is the mechanosensitive triggering of mTORC2 linked to cell migration? One possible route to regulating motility is through altering the dynamics of actin polymerization or myosin contractility (Figure 1A). Earlier studies in neutrophils using partial knockdown of Rictor or mSin1 (using small hairpin RNAs [shRNAs]) have found both positive and negative roles of mTORC2 on cytoskeletal effectors (Rac, Cdc42, RhoA), confounding a clear understanding of the logic of this regulation (Liu *et al.*, 2010; He *et al.*, 2013; Diz-Muñoz *et al.*, 2016). We reasoned that genetic nulls with complete loss of mTORC2-specific subunits in neutrophil-like dHL-60 cells would offer a more surgical approach to dissect these mechanisms, following the success of this strategy in other cell-based models (Guertin *et al.*, 2006; Agarwal *et al.*, 2013; Huang *et al.*, 2017).

To distinguish between the relative contribution of the kinase roles of mTORC2 and the kinase-independent scaffolding roles of Rictor, we devised a CRISPR-Cas9–based approach (Supplemental Figure S1, A and B) to knock out two key components of mTORC2 in dHL-60 cells: its scaffolding subunit Rictor and its kinase accessory subunit mSin1 (Figure 1, B and C). Rictor null (Rictor KO) cells impair both mTORC2 kinase and nonkinase roles, whereas mSin1 null (mSin1 KO) cells specifically affect the kinase roles (Jacinto *et al.*, 2004, 2006; Sarbassov *et al.*, 2004; Guertin *et al.*, 2006). As a pharmacological approach to impair the kinase function of mTOR, we used a specific inhibitor of mTOR kinase KU-0063794 (KU) (García-Martínez *et al.*, 2009). To read out the kinase activity of mTORC2, we assayed the phosphorylation of the well-characterized mTORC2 substrate Akt (Ebner *et al.*, 2017b). When stimulated by chemoattractant peptide formyl-Met-Leu-Phe (fMLP), neutrophil-like differentiated HL-60 (dHL-60) cells derived from both Rictor KO and mSin1KO lines show marked reduction in the phosphorylation of Akt to levels that were comparable to pharmacological inhibition of the mTOR kinase (~75–80% reduction from wild-type [WT] cells; Supplemental Figure S1, C and D), indicating a loss of mTORC2 kinase activity with all of these perturbations.

To determine the importance of these mTORC2 perturbations on cell movement, we performed a transwell chemotaxis assay (Figure 1D), which demonstrated that the perturbations of mTORC2

(WT), Rictor KO, or mSin1 KO cells over a 12-min observation window; axes show *x*-*y* displacement in micrometers. Rictor KO cells migrate poorly and have markedly shorter displacements. (F, G) Box plots (with kernel smooth distribution curve) show mean speed (F) and persistence (G; ratio of displacement/distance) of individual tracks. Both Rictor KO and mSin1 KO cells show a significant reduction ($p < 0.01$; one-way ANOVA with Tukey-means comparison) in migration speed compared with WT. However, only Rictor KO show a significant decrease in the persistence ($p < 0.01$; one-way ANOVA with Tukey-means comparison). $n = 294$ (WT), 138 (RictorKO), and 165 (mSin1 KO) tracks from individual cells pooled across three independent experiments. For box plots, median is indicated by the line, interquartile range (IQR) sets the box width, and error bars indicate 10th–90th percentile. (H) Schematic highlights the phenotypes observed for mSin1 KO and Rictor KO cells. Kinase-dependent roles of mTORC2 appear to regulate speed whereas kinase-independent roles regulate both persistence and speed.

complex formation (in Rictor KO) or kinase activity (in Rictor KO, mSin1KO, or mTOR kinase inhibition) all led to significant and comparable defects in bulk transwell migration (Figure 1D; 60–70% drop in migration index compared with WT). These results agree with earlier reports of chemotaxis defects in Rictor shRNA knockdowns and upon long-term perturbation of mTOR activity with rapamycin (Liu *et al.*, 2010; He *et al.*, 2013; Diz-Muñoz *et al.*, 2016). In addition, we find that both acute (with drug KU) and chronic perturbation (mSin1 KO) of mTOR kinase also impair transwell migration. This is consistent with chemotaxis defects observed in genetic knockouts of Rip3 (Sin1 orthologue of mSin1) in *Dictyostelium* (Lee *et al.*, 2005) but is in contrast with an earlier study using partial knockdown of mSin1 in neutrophils, which found no discernible defects in chemotactic movement of mSin1 KD cells in a microneedle assay (He *et al.*, 2013). Factors like differences in the extent of depletion and the type of migration assay conditions used can often lead to confounding results, so we chose to assess motility defects in cleaner single-cell assays of cell migration with the genetic nulls of mTORC2 components.

We suspected that mTORC2-based mechanoadaptation might be particularly important when cells are in migration environments that mechanically perturb them, including squeezing through a pore for transwell assays or migrating under mild confinement. To study 2D migration under mild confinement, we made use of under-agarose (2% wt/vol) overlay on cells (Bell *et al.*, 2018; Tsai *et al.*, 2019; Brunetti *et al.*, 2022) and tracked individual cells over the course of 20–30 min (assay schematic and cell tracks in Figure 1E) in the presence of uniform chemoattractant (25 nM fMLP). Both Rictor KO and mSin1 KO cells exhibited less net displacement (Figure 1E and Supplemental Figure S2E) and moved at significantly slower speeds (Figure 1F; median speed for Rictor KO: 3.2 μm/min; mSin1 KO: 6 μm/min) compared with WT dHL-60 cells (median speed: 9 μm/min). However, under similar assay environment, only Rictor KO cells showed a significantly reduced persistence (ratio of displacement/distance; median persistence for Rictor KO: 0.1; WT: 0.5), suggesting a role for Rictor beyond the kinase activity of mTORC2. In contrast to the defects observed under agarose, when Rictor KO and mSin1 KO cells were assayed for classical unconfined 2D motility (Supplemental Figure S2A) on glass coverslips coated with fibronectin, they moved with similar displacement, speed, and persistence as WT dHL-60 cells (Supplemental Figure S2, B–D). These results suggest that migratory defects upon mTORC2 perturbation are sensitized in an assay where cells need to actively assess the local environment and adapt during movement. These results also indicate that kinase activity of mTORC2 is specifically required to set the speed of movement, while the scaffolding roles of the complex contribute to maintain persistence of motion (Figure 1H).

Kinase-independent roles of Rictor/mTORC2 restricts the zone of F-actin assembly to the cell front

Persistent motility in neutrophils relies on establishing a single front of lamellipodial F-actin. Earlier studies have shown that fMLP-stimulated neutrophils with reduced levels of Rictor (via shRNA knockdowns) show elevated steady-state levels of F-actin (Diz-Muñoz *et al.*, 2016) with a near-uniform peripheral distribution of actin polymerization (Liu *et al.*, 2010). While this is consistent with Rictor/mTORC2 mediating negative feedback to inhibit F-actin polymerization (Supplemental Figure S1E), the relative contributions of mTORC2 kinase activity and kinase-independent roles in this process remains unclear (Figure 2A). Answering these questions necessitates the larger suite of mTORC2 perturbations that we leverage in the current work.

To assay actin assembly in our mutant backgrounds, we stimulated fibronectin-adhered WT, Rictor KO, and mSin1 KO dHL-60 neutrophils with chemoattractant for 5 min to allow cells to polarize and then fixed and stained them with phalloidin-Alexa647. Consistent with our earlier results (Diz-Muñoz *et al.*, 2016) from partial loss of Rictor (via shRNA knockdowns), Rictor KO cells exhibit significant increase in F-actin levels in polarized cells (Supplemental Figure S1E). In contrast, depletion of mSin1 did not lead to appreciable differences in the F-actin levels compared with WT polarized cells (mSin1 KO; Supplemental Figure S1E), suggesting the kinase arm of mTORC2 may be dispensable for regulating F-actin levels.

Next, we focused on the subcellular features of F-actin distribution in polarized cells after 5 min of chemoattractant stimulation (Figure 2B), visualized via maximum-intensity projections of 3D confocal image stacks. Rictor KO cells showed a broader range of F-actin in the front compared with WT and mSin1 KO cells (Figure 2B). We used linescan (5-μm-line ROI) to measure F-actin levels orthogonal to the leading front (Figure 2C) and fitted the F-actin intensity profile to a bi-Gaussian to estimate the effective width of the F-actin zone (Buys and De Clerk, 1972). While WT and mSin1KO cells have very similar widths of F-actin zone (fitted width ~2–2.5 μm), Rictor depletion led to a twofold expansion of the width of the actin front (fitted width 5.4 μm).

Recent lattice light sheet imaging data have shown that neutrophils generate not only substrate-bound protrusions but also axial protrusions that extend away from the plane of substrate (Fritz-Laylin *et al.*, 2017; Pipathsouk *et al.*, 2021). To investigate whether Rictor/mTORC2 plays a role in constraining the formation and abundance of these axial protrusions, we analyzed the extent of protrusion formation in 3D reconstructions of neutrophils. We used ChimeraX (Pettersen *et al.*, 2021) to 3D reconstruct and render these cells in two axial planes *yz* and *tilted xz* (Figure 2D, ii and iii, and Supplemental Video 1). Confirming our expectation, loss of Rictor led to enhanced accumulation of F-actin–rich protrusions away from the plane of the substrate. These protrusions were frequently present (>50% of all cells imaged; Figure 2E**,** and Supplemental Video 1) in Rictor KO cells, and they were more rarely observed in WT or mSin1 KO cells (~25% of all cells; Figure 2E).

The absence of discernible defects in F-actin distribution in the absence of mSin1 (and hence mTORC2 kinase activity) suggest that mTORC2 relies on its Rictor-dependent kinase-independent signaling to restrict F-actin to the leading edge of cells (Figure 2F). Next, we investigated how mTORC2 regulates the biochemical effectors of front/back polarity in cell motility.

Kinase-independent arm of Rictor/mTORC2 inhibits Rac activity

The migration phenotypes we observe for both kinase-dependent and kinase-independent arms of Rictor/mTORC2 could arise from its engagement with different portions of the migration cascade (Figure 3A). A wide range of motile cells including neutrophils show a distinct front-back polarity and organize their protrusive fronts and contractile backs using Rac and RhoA/myosin signaling, respectively (Xu *et al.*, 2003). We were interested in how mTORC2 regulates these polarity and cytoskeletal programs. Cellular stretch has been shown to inhibit Rac activity in several contexts (Katsumi *et al.*, 2002; Houk *et al.*, 2012), but it is not clear which arm of mTORC2 activities is necessary for this inhibition in neutrophils.

Here, we probed whether kinase activity of mTORC2 is dispensable restricting Rac activation and actin polymerization (Figure 3A). To investigate mTORC2 regulation of Rac, we leveraged a

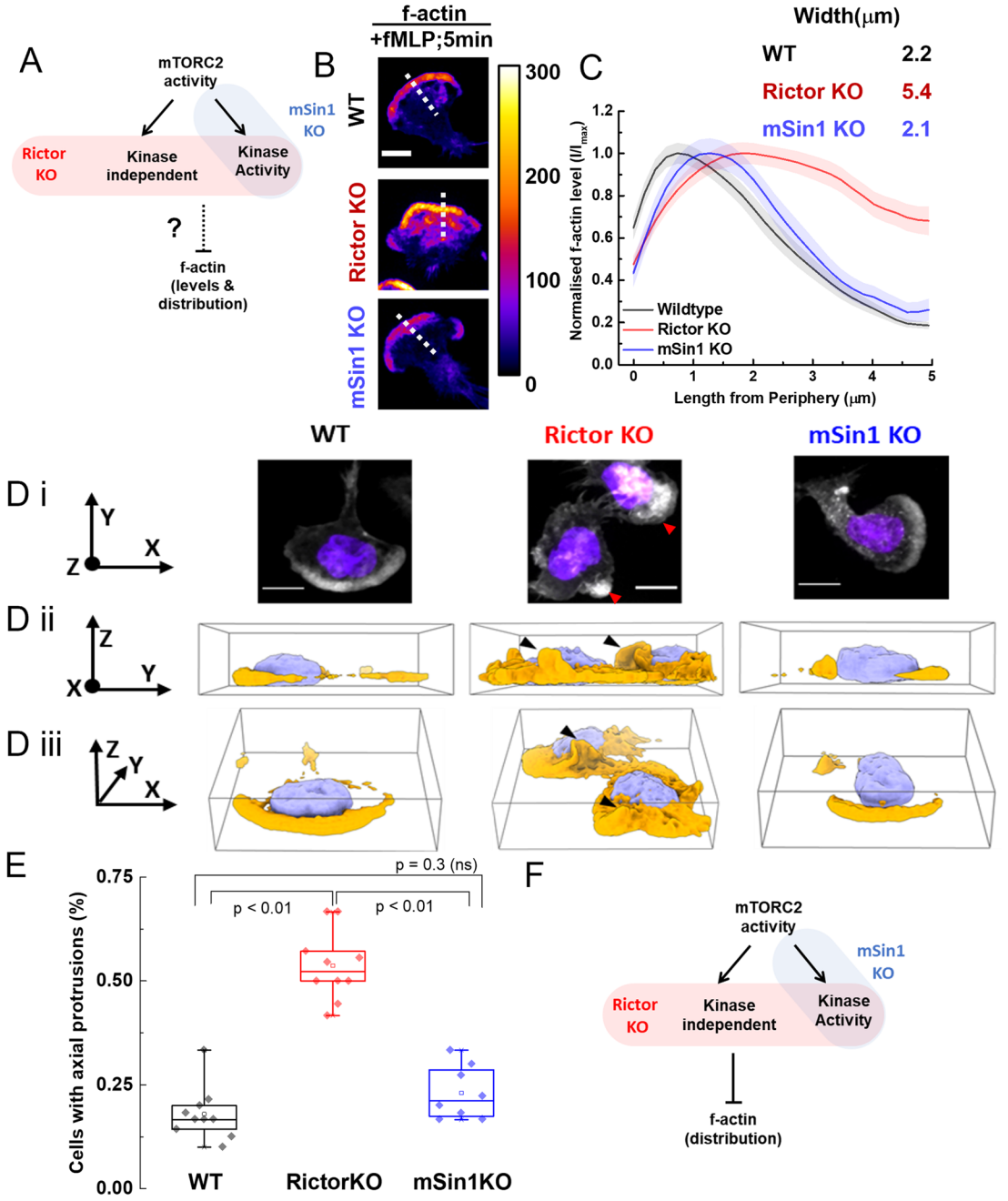

FIGURE 2: Kinase-independent arm of Rictor/mTORC2 restricts the zone of F-actin assembly to the front of the cells. (A) Schematic shows how we are probing the kinase-dependent vs. independent roles of mTORC2 in regulating F-actin levels and spatial organization. (B) Maximum intensity projections of Alexa647-phalloidin stained F-actin obtained from confocal z-stacks (10 μm in z-depth) for WT, Rictor KO, or mSin1 KO dHL60 cells, 5 min after stimulation with 25 nM fMLP. Fire-LUT shows the intensity scaling; scale bar 10 μm. (C) F-actin intensity (normalized to individual peak) line scans (mean ± SEM) obtained (dashed lines on B) from WT ($n = 35$), Rictor KO ($n = 48$), or mSin1 KO ($n = 26$) dHL60 cells pooled from two independent experiments. Rictor KO (red) has a wider lateral zone of leading-edge F-actin in comparison to WT (black) and mSin1 KO (blue); quantified by bi-Gaussian fitting of the intensity profile. (D) Representative WT, Rictor KO, and mSin1 KO dHL60 cells shown as either maximum intensity projection (D i; *xy* plane; scale bar 10 μm); or a ChimeraX 3D reconstruction in *yz* plane (D ii) and a tilted *xz* plane (D iii) to highlight the axial features of F-actin (gold) distribution and nucleus (blue) as reference. Rictor KO cell shows protrusions out of the plane of the substrate that are rarely present in either WT or mSin1 KO cells. (E) Box plots quantify fraction of cells with axial protrusions obtained from ChimeraX 3D-reconstruction views of each cell type (~10 fields; at least 100 cells analyzed for each condition) across two independent experiments. RictorKO cells have significantly ($p < 0.01$; one-way ANOVA with Tukey's mean comparison test) higher fraction of cells with axial protrusions. For box plots, median is indicated by the line, interqurtile range sets the box width, and error bars indicate 10th–90th percentile. (F) Defects observed in F-actin distribution for only RictorKO dHL60 cells but not mSin1 KO cells suggests a kinase-independent arm of Rictor/mTORC2 is required for negative feedback on F-actin assembly, distribution, and organization.

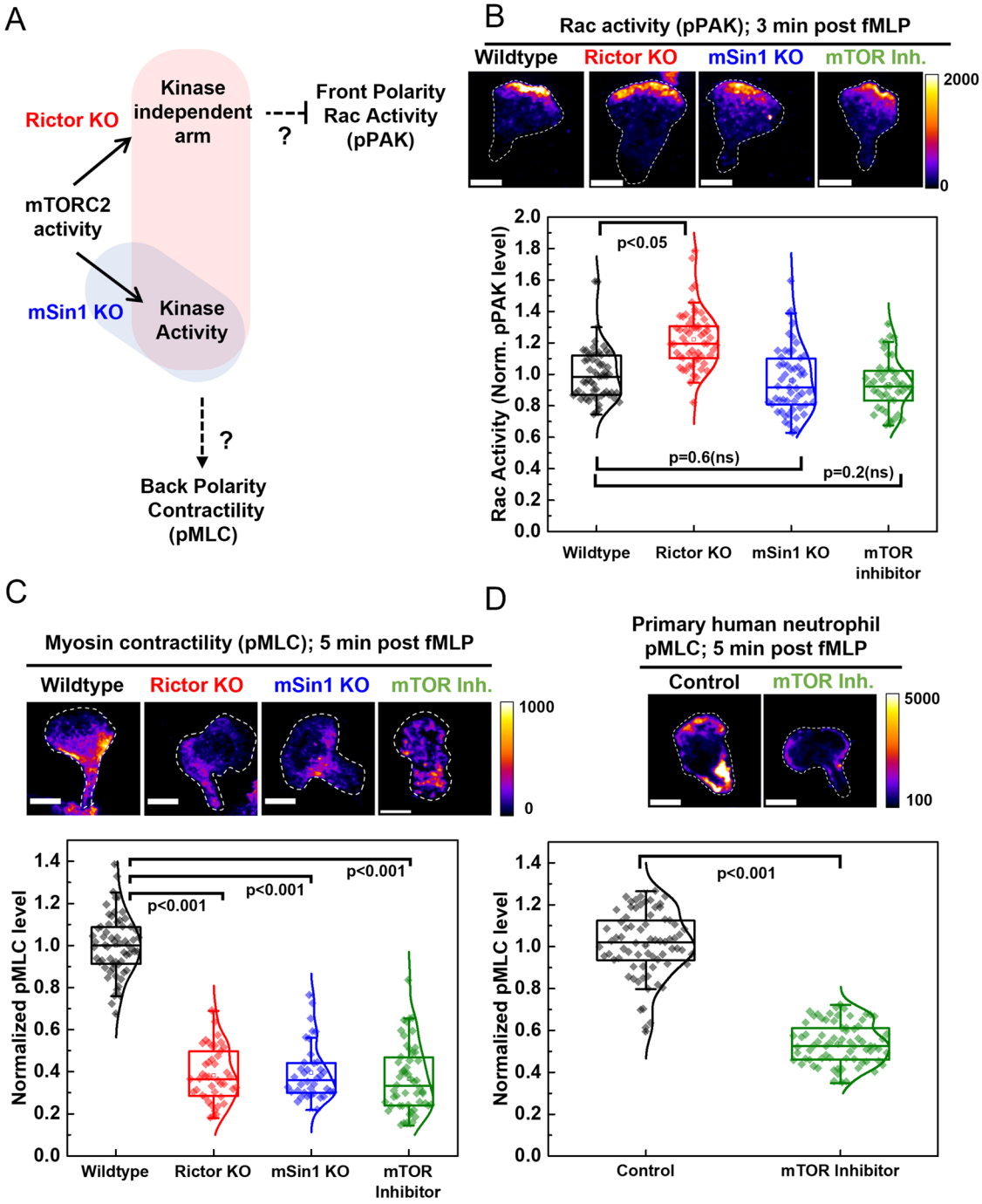

FIGURE 3: Kinase-independent arm of Rictor/mTORC2 inhibits Rac activity while its kinase role stimulates myosin contractility. (A) Schematic shows how we probe the kinase-dependent vs. independent roles of mTORC2 in regulating front (Rac activity) and back (myosin contractility) polarity programs. (B) Phospho-PAK (pPAK) immunostaining (labeled with Alexa 488 secondary antibody) of WT, Rictor KO, mSin1 KO, and WT cells treated with mTOR Inhibitor (10 μM KU) adhered to fibronectin-coated glass; 3 min after stimulation with 25 nM fMLP. Box plots show the quantification of total pPAK intensity levels normalized to WT population from confocal z-stacks as shown above (40–50 fields and at least 300 cells for each condition) pooled from four independent experiments. Only Rictor KO cells exhibit significantly elevated pPAK levels compared with WT cells ($p < 0.05$; one-way ANOVA with Tukey's mean comparison test). (C) Phospho-myosin light chain (pMLC) immunostaining (labeled with Alexa 488 secondary antibody) of WT, Rictor KO, mSin1 KO, and WT cells treated with mTOR inhibitor (10 μM KU) adhered to fibronectin-coated glass; 5 min after stimulation with 25 nM fMLP. Box plots show the quantification of total pMLC intensity levels normalized to WT population from confocal z-stacks as shown above (30–50 fields and at least 300 cells across each condition) pooled from three independent experiments. Perturbation of mTORC2 kinase activity in Rictor KO, mSin1 KO, and upon mTOR inhibition led to a profound decrease in pMLC levels compared with WT cells ($p < 0.001$; one-way ANOVA with Tukey's mean comparison test), suggesting that the kinase activity of Rictor/mTORC2 stimulates myosin contractility. (D) pMLC immunostaining of primary human neutrophils, either untreated (control) or mTOR inhibited (10 μM KU) adhered to

quantitative immunofluorescence assay to probe Rac activity following the phosphorylation profile of Rac effector p21-activated kinase (Pak) upon chemoattractant stimulation (Itakura *et al.*, 2013; Graziano *et al.*, 2019). Although chemoattractant (fMLP) addition is sufficient to trigger downstream signaling and polarization of neutrophil-like dHL-60 cells in suspension and is often used to assay Rac activity biochemically, we chose to carry out these assays on cells adhered to fibronectin-coated glass (Itakura *et al.*, 2013). This approach enabled improved imaging for quantification and reliable comparison of the effects of mTORC2 perturbations using cells treated and plated in similar conditions (Figure 3, B and C, and Supplemental Figure S3, C and D). Cells from all conditions (WT, Rictor KO, mSin1 KO, and mTOR inhibited WT) were able to polarize and organize Rac activity (pPAK) at the leading edge after 3 min of chemoattractant stimulation (Figure 3B). Rictor KO cells exhibited elevated levels (~20–25% above WT) of sustained Rac activity. In contrast, perturbation of mTORC2 kinase activity (in mSin1 KO cells or upon mTOR kinase inhibition with KU) did not significantly alter Rac activation. We independently verified these results with alternate KO clones of Rictor and mSin1 targeting other genomic regions (Supplemental Figure S3, A and B) and found Rac activity elevated in the alternate Rictor KO clone but not mSin1 KO clone (Supplemental Figure S3C). The marked differences in Rac activity observed upon interfering with the kinase-independent (Rictor KO) but not the kinase-dependent arms of mTORC2 (mSin1 KO or mTOR kinase inhibition) suggests that the kinase-independent roles of Rictor/mTORC2 are responsible for limiting leading-edge Rac signals.

mTORC2 kinase activity stimulates myosin contractility at the trailing edge

Next, we investigated whether perturbation of mTORC2 activity also affects polarity signaling at the trailing edge of the cell. Active RhoA and its associated RhoA-kinase localize and phosphorylate myosin regulatory light chain (pMLC) to power contraction of the trailing edge (Wong *et al.*, 2006; Tsai *et al.*, 2019). Biochemical studies in neutrophils have shown that mTORC2 kinase effector PKC regulates RhoA and myosin activity in neutrophils (Liu *et al.*, 2010, 2014). If kinase roles of mTORC2 stimulate myosin contractility, we expect both Rictor KO and mSin1 KO cells to show reduced pMLC levels (Figure 3A). If the RhoA/myosin inhibition is secondary to an increase in the antagonistic Rac activation, we would expect larger effects for Rictor KO cells.

We used immunofluorescence (IF) against phospho-MLC to probe myosin contractility in dHL-60 neutrophils plated on glass and stimulated with chemoattractant (25 nM fMLP) for 5 min to allow cells to polarize (images; Figure 3C). We find all three conditions (Rictor KO, mSin1 KO, and mTOR inhibition using KU) lead to profound loss of pMLC activation (~50–60% reduction; Figure 3C). We verified these results independently with alternate KO clones of Rictor and mSin1, which both showed similar reduction in pMLC levels (Supplemental Figure S3D). Finally, we extended these analyses to primary human neutrophils where we can inhibit mTOR kinase activity with KU and assay pMLC level using similar assay condition and readouts as dHL-60 cells (Figure 3D). Experiments in primary human neutrophils confirmed that mTOR kinase inhibition also leads to a profound decrease (~40–50%) of pMLC upon chemoattractant stimulation.

In summary, our results show that the kinase-independent roles of Rictor/mTORC2 inhibit Rac activity in the front, while the kinase roles of mTORC2 stimulate contractility at the back, potentially enabling the two divergent downstream arms of mTORC2 to independently regulate the front and back polarity programs. We next explore the consequence of this regulatory circuit for front-back polarity coordination during motility.

Rictor/mTORC2 spatially and temporally coordinates the front and back polarity program during movement

Migrating neutrophils rely on front-back polarity coordination to persistently move, turn, and reorient during migration. This front-back coordination depends on multiple currencies including cell membrane tension (Houk *et al.*, 2012), actin flows (Maiuri *et al.*, 2015), myosin contractility (Tsai *et al.*, 2019), and biochemical signaling crosstalk (Xu *et al.*, 2003; Ku *et al.*, 2012) between the front and back polarity programs. Our results (Figure 3) suggest that neutrophils leverage the two arms of mTORC2 downstream signaling to coordinate front and back polarity signaling. We asked whether this logic contributes to the spatial organization and temporal coordination of polarity during movement (Figure 4, and Supplemental Figures S4 and S5).

To investigate the role of mTORC2 in front/back coordination, we revisited the agarose overlay conditions (Bell *et al.*, 2018; Brunetti *et al.*, 2022) that sensitized Rictor-dependent migratory phenotypes (Figure 1, E–G). To map the distribution and coordination of polarity in migrating cells, we coexpressed localization biosensors for both active Rac (from Pak; Srinivasan *et al.*, 2003) and active RhoA (from Anilin; Piekny and Glotzer, 2008) in WT and Rictor KO cells and imaged them at high spatial and temporal resolution (frame interval of 3 s) in the presence of uniform chemoattractant 25 nM fMLP (Figure 4, A and B montage, and Supplemental Video 2). First, we assessed the spatial features of front and back regulation in these cells. Active Rac forms a gradient in the front half of a polarized WT cell, while active RhoA is tightly focused at the rear (Figure 4A; WT). A linescan in the direction of cell movement (front-back axis) reveals the mutually exclusive distribution of the biosensor and a strong anti-correlation (Pearson's $R = -0.49$ for WT; Figure 4C). Although Rictor KO (Figure 4B) and mSin1 KO (Supplemental Figure S5A**)** cells also polarize, they do so with an elongated stalk at the cell back (arising from low contractility), where the bulk of RhoA biosensor fluorescence is concentrated. However, WT and mSin1 KO cells showed strong mutual antagonism of Rac and RhoA, with RhoA activity completely excluded from the Rac-positive zones in the cell front (Figure 4C and Supplemental Figure S5B). In contrast, Rictor KO cells showed local hotspots of RhoA biosensor localization in the cell front (Figure 4D). This impaired spatial sorting of front and back polarity signals can be detected by poor anti-correlation between both biosensors (Pearson's $R = -0.22$ for Rictor KO; Figure 4D). Front-back correlation (Figure 4E) quantified from several cells (WT = 23 cells, Rictor KO = 33 cells, and mSin1 KO = 20 cells) shows

fibronectin-coated glass; 5 min after stimulation with 25 nM fMLP. Box plots show profound reduction total pMLC intensity levels in mTOR inhibited cells normalized to control population (~70 fields and at least 500 cells for both conditions; $p < 0.001$ by Mann-Whitney test) pooled from three independent experiments and healthy volunteers. All representative images (B–D) show maximum-intensity projections obtained from 10 μm z-depth confocal z-stacks; scale bar 10 μm. Dashed outlines indicate the cell boundary, and all conditions were equally intensity scaled as shown by associated Fire LUT. For all box plots (B–D), median is indicated by the line, interquartile range sets the box width, and error bars indicate 10th–90th percentile.

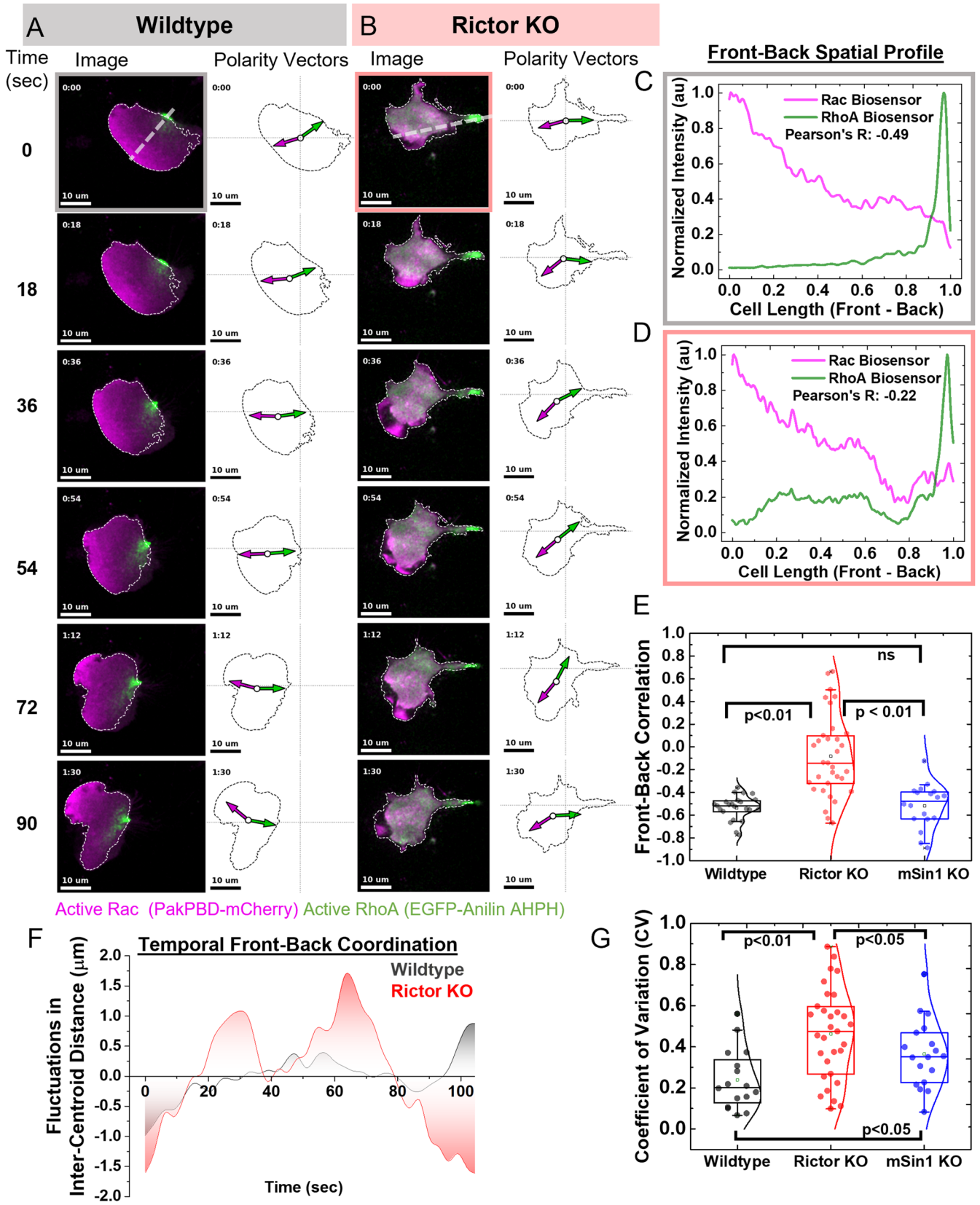

FIGURE 4: Rictor/mTORC2 is required for maintaining the spatial and temporal coordination of the front and back polarity programs. (A) Wildtype (WT) and Rictor KO (B) cells coexpressing Rac biosensor (Pak-PBD-mCherry) and RhoA biosensor (EGFP-anillin-AHPH) were plated under 2% agarose overlay and imaged every 3 s using a confocal spinning-disk microscope. Montage of images acquired over 90 s show the distribution of front (active Rac; magenta) and back (active RhoA; green) polarity signals (image, left) and the corresponding front (magenta arrow) and back (green arrow) polarity vectors. The cell centroid for each frame is indicated by the open circle and its displacement from the grid

significantly elevated correlation values thereby suggesting poorer front/back separation (median for WT = –0.55, Rictor KO = 0.1, and mSin1 KO = –0.5). These defects originate specifically from differences in biosensor distribution across the front-back axis, as lateral linescans perpendicular to the direction of movement (Supplemental Figure S4, A and B, and S5C) do not show any preferential bias and resulted in similar overall distribution of Pearson correlation across the lateral plane for WT, Rictor KO, and mSin1 KO cells (Supplemental Figure S4C).

Next, we probed the temporal coordination of front-back polarity during movement under agarose. Recently, we used a polarity metric based on the centroid of biosensor intensity with respect to the geometric centroid of the cells to monitor Rac polarity (Graziano *et al*., 2019). We revised this analysis approach to compute the centroid of biosensor intensities for both the Rac and RhoA biosensor (polarity vectors for WT and Rictor KO in Figure 4, A and B). The distance between the zones of Rac and RhoA activation (intercentroid distance) provides a measure of separation between front and back signals during migration (length between arrowheads of polarity vectors for WT and Rictor KO in Figure 4, A and B). Cells proficient in coordinating front-back polarity during persistent movement exhibit smaller fluctuations in intercentroid distance (WT in Figure 4F). Rictor KO cells show enhanced amplitude of fluctuations for front/back separation (Figure 4F). We quantified the strength of these fluctuations as coefficient of variation (CV), a commonly used metric to quantify fluctuations in cell polarity (Lai *et al*., 2018; Onwubiko *et al*., 2019). Loss of Rictor leads to a stronger phenotype and significant increase in CV (Figure 4G; median CV for WT: 0.2, Rictor KO: 0.5, and mSin1 KO: 0.35) while mSin1KO cells also exhibit a modest phenotype in front-back coordination. These results indicate that loss of Rictor can perturb both kinase-dependent and independent arms of mTORC2, which allow coordination between the polarity signals at front and back.

Our experiments probe how different branches downstream from mTORC2 activation (kinase dependent vs. independent) relate to regulation of front-back polarity programs and their spatiotemporal coordination during movement. We next investigated whether biochemical signals and physical forces synergize to active mTORC2 in the first place.

Mechanical stretch synergizes with PIP_3 generation to activate mTORC2

TORC2 is an ancient program that has been shown to be regulated by both biochemical and mechanical inputs in several contexts ranging from yeasts to *Dictyostelium* to immune cells. Although mechanical stretch is one important regulator of the activation of the complex in *Dictyostelium*, mounting evidence suggests biochemical inputs from Ras (and Rap) are required for full activation of the complex (Artemenko *et al*., 2016; Khanna *et al*., 2016). We have previously shown mechanical stretch can activate mTORC2 activity in neutrophils (Diz-Muñoz *et al*., 2016). Here, we carry out a more systematic analysis of whether mechanics synergizes with biochemical inputs (as likely to happen in cells) to robustly amplify mTORC2 signaling outputs. To investigate whether mechanical stretch suffices to activate the mTORC2 complex, we exposed neutrophils to hypotonic media (50% decrease in ionic strength) and assayed the activation of mTORC2 via Akt phosphorylation. Hypotonic exposure (purely mechanical input) stimulates modest levels of mTORC2 activity, much less compared with purely chemoattractant stimulation (Figure 5, B and C). Surprisingly, hypotonic exposure paired with chemoattractant addition (combination of biochemical and mechanical inputs) can robustly activate mTORC2 and amplify (approximately twofold) its signaling output (Figure 5, B and C). These results suggest that mechanical stretch from PM synergizes with other biochemical inputs from chemoattractant to amplify mTORC2 signaling activity.

Chemoattractant fMLP activates a wide range of downstream signaling pathways (Gβγ, PI3K, Ras; Xu *et al*., 2003). Which of these programs are necessary to synergize with mechanical inputs to amplify mTORC2 outputs? Here we focused on the PI3K node that is responsible for PI-3,4,5-P_3 (PIP_3) generation at the front of the cells. PIP_3-Rac-positive feedback is central for instructing actin polymerization in the front and raising cellular tension (Wang *et al*., 2002; Weiner *et al*., 2002). Moreover, PIP_3 is also responsible for recruitment of mTORC2 phospho-substrate Akt (Ebner *et al*., 2017a,b). In neutrophils, PI3Kγ is the dominant regulator of fMLP-dependent PIP_3 production (Stephens *et al*., 1994; Hannigan *et al*., 2002). To test whether PI3Kγ activity is necessary for stretch-dependent amplification of mTORC2 activity, we used PIK90 (Van Keymeulen *et al*., 2006), a specific inhibitor of PI3Kγ (Figure 5D). dHL-60 cells

indicates overall cell movement; scale bar 10 μm. (C, D) Anti-correlation between the intensity profile of polarity signals across the front-back axis provides a measure of spatial segregation of the front-back signals. Representative intensity profiles of Rac and RhoA biosensors obtained from line scan (dashed line in time 0 s in A and B) of WT (C) and Rictor KO (D), with computed Pearson's correlation coefficient for each set of intensity traces (Pearson's correlation coefficient = –0.49 for WT; –0.22 for Rictor KO). Lower Pearson's correlation coefficient indicates better separation between front and back signals. (E) Box plots of front-back correlation values for WT ($n = 23$ cells), Rictor KO cells ($n = 33$ cells), and mSin1 KO cells ($n = 20$ cells) pooled from four independent experiments. Rictor KO cells have significantly higher correlation coefficient ($p < 0.01$; one-way ANOVA with Tukey's mean comparison test) compared with both WT and mSin1 KO cells suggesting impaired spatial sorting of front-back polarity programs. (F) To measure the extent of temporal coordination between polarity signals, we analyzed the fluctuations in the weighted intercentroid distance between the front and back polarity biosensor intensities (indicated by the distance between the arrowheads of polarity vector in images A and B). WT cells have polarity vectors uniformly aligned to the front-back axis and maintain a stable intercentroid distance (gray), while Rictor KO cells show stronger fluctuations in intercentroid distance (red). Representative plot of fluctuations in intercentroid distance for both cell types of WT and Rictor KO. We use coefficient of variation (CV) as a metric to quantify the magnitude of the fluctuations. (G) Box plots of distribution of CV obtained for WT ($n = 19$ cells), Rictor KO ($n = 30$ cells), and mSin1 KO cells ($n = 16$ cells) across four independent experiments. Rictor KO cells exhibit significantly ($p < 0.01$) higher fluctuations in ICD compared with both WT cells, while mSin1 KO cells also exhibit a modest yet statistically significant ($p < 0.05$) phenotype. All statistical comparisons were done by one-way ANOVA with Tukey's mean comparison test. These results suggest impaired temporal coordination of front and back polarity programs in mTORC2 perturbed cells. For box plots, median is indicated by the line, interquartile range sets the box width, and error bars indicate 10th–90th percentile.

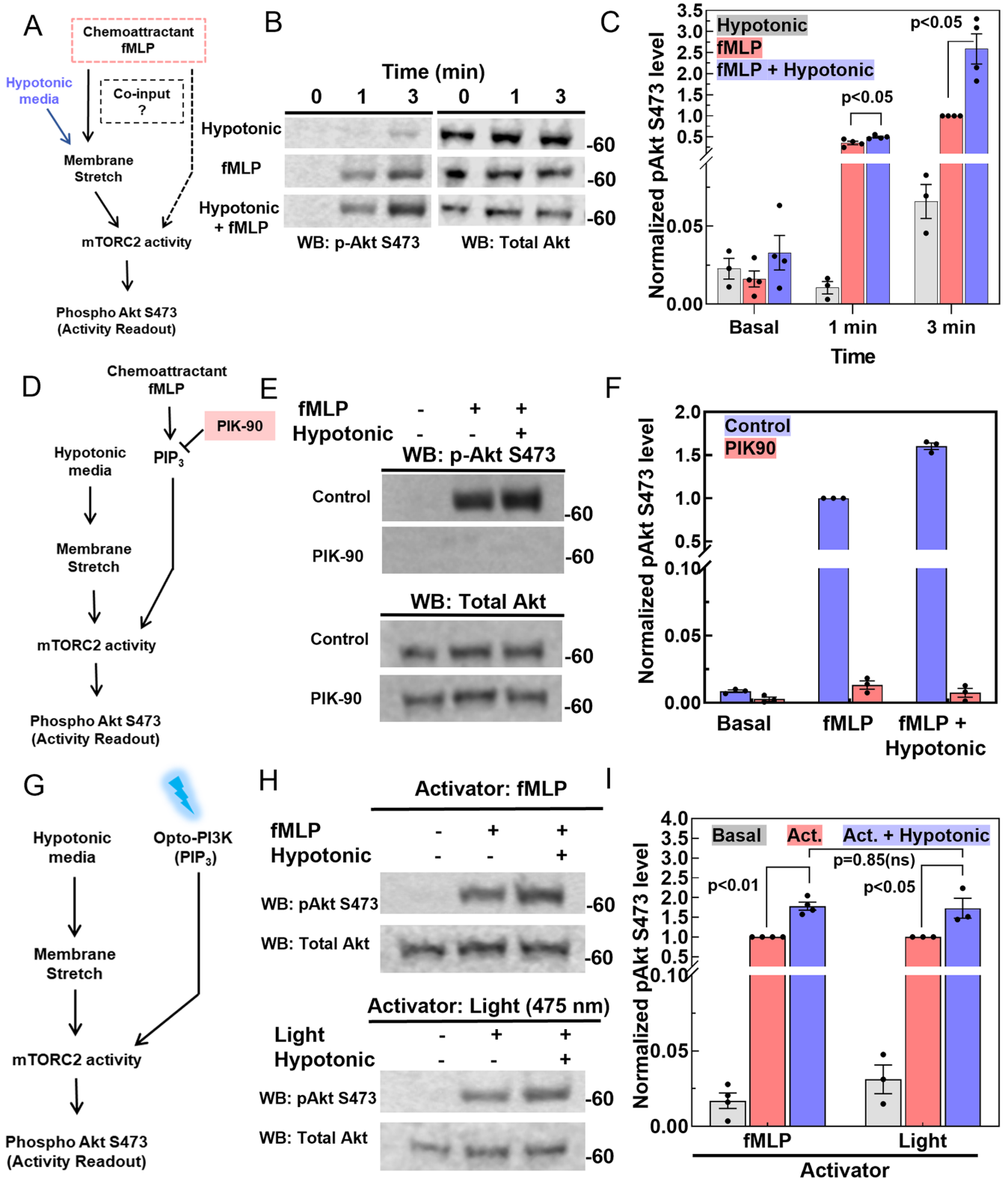

FIGURE 5: Mechanical stretch synergizes with PIP_3 generation to amplify mTORC2. (A) Probing whether mTORC2 activation can be amplified by a combination of mechanical stretch (here applied by 50% hypotonic shock) and additional biochemical inputs downstream from chemoattractant fMLP stimulation. (B) To probe the logic of mTORC2 activity amplification, dHL-60 cells were subjected to either just hypotonic media (50% osmolarity reduction), stimulated with 100 nM fMLP (fMLP only), or subjected to both inputs (hypotonic + 100 nM fMLP). mTORC2 activity was assayed in basal (0 min) and different time points (1 and 3 min) using phospho-Akt S473 and pan-Akt immunoblots, and representative immunoblot panels are shown. (C) mTORC2 activity (pAkt/panAkt ratio) was quantified and normalized to 3 min fMLP condition for each experiment; plotted as mean ± SEM from three independent experiments. Hypotonic

pretreated with PIK90 and subsequently stimulated with fMLP alone or in combination with hypotonic media (50% osmolarity) show background (basal) levels of pAkt in immunoblots compared to untreated cells (Figure 5, E and F). These results show that PI3Kγ-induced PIP_3 synthesis is necessary for neutrophils to activate and amplify mTORC2 kinase activity upon osmotic stretch.

Finally, we tested whether PIP_3 is sufficient to replace chemoattractant in mechanics-synergized mTORC2 activation. For this purpose, we used an optogenetic module (Opto-PI3K) that can synthesize PIP_3 in response to light stimulation (Figure 5G; Graziano *et al.*, 2017). Optogenetic stimulation of PIP_3 sufficed as the co-input with mechanical stretch in mTORC2 activation (Figure 5, H and I). Our results indicate that PIP_3 and mechanical stretch jointly drive robust amplification of mTORC2 activity.

DISCUSSION

For persistent motility, neutrophils must coordinate the activation of their leading and trailing cytoskeletal networks (Houk *et al.*, 2012; Tsai *et al.*, 2019). The mTORC2 complex is a critical regulator of this coordination. Following protrusion-induced membrane stretch, mTORC2/Rictor activation inhibits actin polymerization to enable a dominant front to emerge (Diz-Muñoz *et al.*, 2016) and regulates myosin contractility at the trailing edge (Liu *et al.*, 2010). Here we use a combination of genetic nulls and pharmacological tools to investigate the kinase-dependent and independent links from mTORC2 to these cytoskeletal programs. mTORC2 is indispensable for movement when neutrophil-like dHL-60 cells are mildly confined (~5 μm) under agarose to mimic the confined spaces these cells explore in vivo (Figure 1). The kinase-independent roles of Rictor/mTORC2 are central to regulating the leading-edge polarity program (Rac activity, F-actin distribution; Figures 2 and 3) while its kinase activity stimulates myosin contractility at the trailing edge. Using dual biosensor imaging of the front and back polarity program, we show that mTORC2 is necessary for the spatial and temporal coordination of polarity during movement (Figure 4). Finally, we probe the requirements for mTORC2 activation. Membrane stretch synergized with the biochemical input PIP_3 to amplify mTORC2 activity (Figure 5). In summary, our results highlight the logic of stretch-activated Rictor/mTORC2 signaling in coordinating front-back polarity during neutrophil movement (working model in Figure 6).

TORC2 is an ancient regulator of PM tension homeostasis across evolution (Eltschinger and Loewith, 2016; Riggi *et al.*, 2020). In yeasts, an increase in PM tension triggers TORC2-based homeostatic responses to increase the surface area of the plasma membrane (Berchtold *et al.*, 2012; Riggi *et al.*, 2018). In *Dictyostelium*, the TORC2 signaling program is activated by shear stress and regulates polarity, chemotaxis, and electrotaxis (Lee *et al.*, 2005; Kamimura *et al.*, 2008). In neutrophils, disruption of mechanosensory mTORC2 leads to elevated levels of membrane tension arising from increased actin polymerization (Diz-Muñoz *et al.*, 2016). Among other immune cells, loss of Rictor in B cells dramatically increases cortical F-actin levels following B-cell receptor stimulation (Huang *et al.*, 2017). Similar mechanisms could also restrict actin polymerization at the tip of the leading edge of oligodendrocytes as they wrap around the axonal shaft during myelin sheath formation (Bercury and Macklin, 2015; Nawaz *et al.*, 2015), as mTORC2 signaling has been shown to regulate the differentiation, shape, and actin cytoskeleton organization of these cells (Bercury *et al.*, 2014).

How does mTORC2 interface with cell polarity? While the kinase-independent roles of Rictor/mTORC2 inhibits the front (Rac), its kinase activity stimulates the back (RhoA). Using two distinct aspects of mTORC2 potentially enables independent regulation of the spatially polarized front and back program. Further, the use of a shared signaling node of mTORC2 activation may help facilitate coordination between the two polarity programs (Figure 6). This mTORC2-based mechanism of signaling-based coordination between the two programs is likely to operate in conjunction with the recently reported fast mechanical coupling of protrusion and retraction dynamics observed in both neutrophils (Tsai *et al.*, 2019) as well as other cells that undergo ameboid migration (Liu *et al.*, 2015; Maiuri *et al.*, 2015).

How are downstream arms of Rictor/mTORC2 linked to regulation of front/back polarity signals? We show that the kinase-independent arm of Rictor/mTORC2 inhibits Rac activation and actin polymerization at the leading edge (Figures 2 and 3) consistent with

shock (gray bars) alone stimulates very low levels of mTORC2 activity (gray bar), and chemoattractant addition is needed to trigger robust activation of signaling (red bar). However, a combination of fMLP and hypotonic shock (blue bar) significantly amplifies the signaling output of mTORC2 ($p < 0.05$, unpaired *t* test). Each bar represents mean ± SEM from three independent experiments. (D) Probing the necessity of chemoattractant-driven PIP_3 generation (using PI3Kγ inhibitor PIK-90) for synergistic amplification of mTORC2 activity upon hypotonic shock. (E) Representative immunoblots of pAktS473 and pan-Akt to measure mTORC2 activation. Control (top) or PIK-90 (1 μM; bottom) treated dHL60 cells were assayed for mTORC2 activity in the absence (basal activity; –/– condition; left lane) or in the presence of fMLP alone (+/–; middle lane) or a combination of fMLP and hypotonic shock (+/+; right lane). In the presence of PIK-90, mTORC2 activity is severely attenuated (with background levels of pAkt S473 detected). (F) mTORC2 activity (pAkt/panAkt) was quantified across the three conditions and normalized to control (fMLP alone) for each experiment; plotted as mean ± SEM from three independent experiments. The profound reduction of mTORC2 signaling output upon inhibition of PI3K activity suggests PIP_3 is a *necessary* co-input for activation (fMLP) and amplification of mTORC2 activity upon stretching (fMLP + hypotonic). (G) Testing whether PIP_3 (via optogenetic activation) is sufficient to activate mTORC2 and can collaborate with mechanical stretch to amplify mTORC2 activation. (H) Representative immunoblots of pAktS473 and pan-Akt of dHL60 cells activated either with chemoattractant (20 nM fMLP for 3 min; top panel) or using light at 475 nm (~1 mW power for 3 min) to activate Opto-PI3K (bottom panel). For both inputs, pAkt/pan-Akt was assayed for basal (left lane; –/–), just stimulus (middle lane; +/–), or when paired with hypotonic media (right lane; +/+). (I) mTORC2 activity (assayed by pAkt/AKT ratio) quantified across the three different conditions (H) for both activator (fMLP or light) and normalized using the activator-only condition (just fMLP or light) for each experiment; plotted as mean ± SEM from three independent experiments. mTORC2 signaling activity is significantly boosted upon hypotonic shock ($p < 0.01$ for fMLP; $p < 0.05$ for Light; both by unpaired *t* test) with similar extent of amplification observed when either fMLP or Opto-PI3K was used as activator ($p = 0.85$; ns; unpaired *t* test). This indicates PIP_3 generation is *sufficient* to synergize with mechanical stretch to amplify mTORC2 activity.

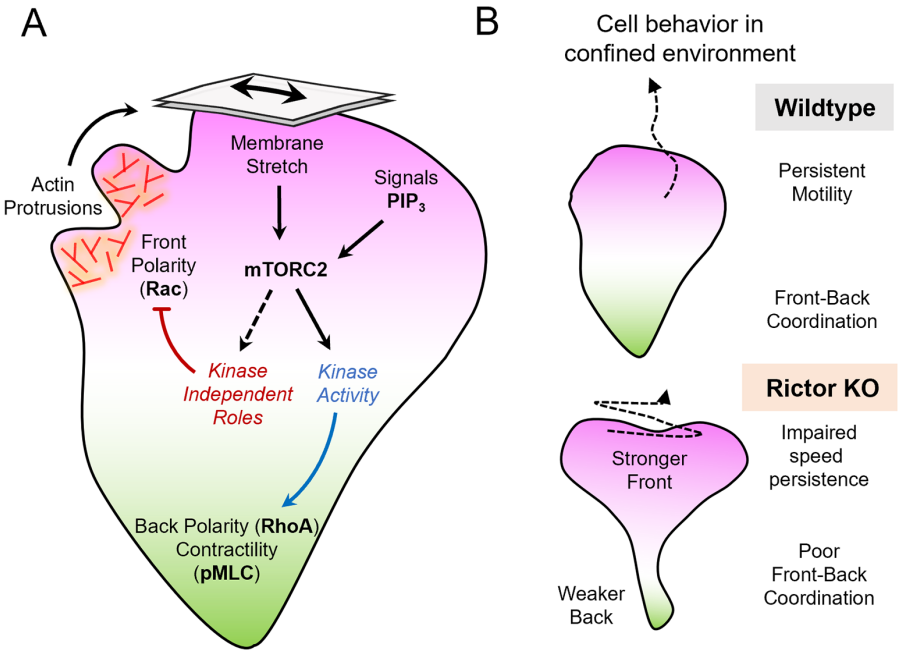

FIGURE 6: Working model for the molecular logic of mTORC2-based regulation of front and back cytoskeletal programs. (A) Membrane stretches and biochemical signals from PIP3 synergize to activate mTORC2 signaling programs and drive robust amplification of its kinase activity output. Noncatalytic kinase-independent roles of Rictor/mTORC2 (black dashed arrow) allow stretch-dependent inhibition of front polarity signals (Rac) and restrict F-actin protrusion to the leading edge. The kinase roles of mTORC2 are necessary to stimulate myosin contractility (pMLC) at the back. While the spatial logic and molecular details of this circuit remains poorly understood, our results suggest this bifurcation of the downstream mTORC2 activities enables independent regulation of the spatially polarized front (magenta) and back (green) programs. (B) The regulatory circuit for mTORC2-based front-back coordination (A) is essential for persistent movement in confined environments where cells experience mechanical stretch (like under agarose). In the absence of mTORC2 activities (as in Rictor KO), cells exhibit elevated Rac activity (Stronger Front) and lowered contractility (Weaker Back); consequently, front-back coordination is lost resulting in impaired speed and persistence of motility in confined environment.

some (Diz-Muñoz *et al.*, 2016) but not all (He *et al.*, 2013) previous studies, possibly owing to differences between the use of mTORC2 subunit knockdowns in previous work and complete knockouts in the present work. There are a number of potential mechanistic links from Rictor/mTORC2 to Rac activation. mTORC2 has been shown to directly interact with Rac1 (Saci *et al.*, 2011) and regulate Rac GEFs P-Rex1 and Tiam1 (Hernández-Negrete *et al.*, 2007; Morrison Joly *et al.*, 2017). Some of the kinase-independent roles of mTORC2 could also arise from the scaffolding roles of Rictor independent of mTORC2 (Agarwal *et al.*, 2013; Gkountakos *et al.*, 2018). For instance, Rictor participates in mTOR-independent scaffolding complex with the unconventional Myo1c in adipocytes to regulate membrane ruffing (Hagan *et al.*, 2008), whose hematopoietic isoform Myo1g is a key regulator of cellular surface topology and membrane tension in other immune cells (Gérard *et al.*, 2014).

We find the kinase activity of mTORC2 *positively* regulates myosin contractility and tail retraction (Figures 3 and 4). Our results are not consistent with an earlier study in neutrophils that had linked mTORC2-dependent phosphorylation of PKCβII to cAMP-based *inhibition* of RhoA/pMLC activity (Liu *et al.*, 2010, 2014). This discrepancy could arise from the partial knockdown of a single subunit (Rictor by shRNA) analyzed in the previous study, while in this study we have analyzed independent clonal knockout lines for two subunits (Rictor and mSin1) as well as pharmacologically inhibited mTOR kinase activity in both HL-60 neutrophil-like cells and primary human neutrophils to verify the positive link from mTORC2 kinase activity to pMLC (Figure 3 and Supplemental Figure S3). Our results are consistent with earlier studies in *Dictyostelium*, where both Pia (Rictor) null and Rip3 (Sin1) null showed a marked reduction in chemoattractant-induced myosin assembly (Lee *et al.*, 2005). Moreover, the mTORC2 phospho-substrate PKC has been shown to increase myosin II contractility in neuronal growth cones (Yang *et al.*, 2013). Future work will identify the molecular players that act downstream from mTORC2 to regulate front-back polarity signals.

mTORC2 activation integrates several upstream inputs like chemoattractant, growth factors, Ras, and mechanical forces (Diz-Muñoz *et al.*, 2016; Khanna *et al.*, 2016; Kovalski *et al.*, 2019). In *Dictyostelium*, TORC2 activation relies on inputs from other leading-edge components including Ras and Rap GTPase (Khanna *et al.*, 2016; Senoo *et al.*, 2019). We find that osmotic stretch can significantly amplify the signaling output of chemoattractant-stimulated kinase activity of mTORC2. PI3K activity is necessary and sufficient for this amplification (Figure 5). Our results suggest that a combination of biochemical inputs and mechanical stretch can combine to trigger mTORC2 activity to inhibit actin assembly in protrusions that also contain the biochemical co-input PIP_3. PIP_3 could play this positive role by the joint recruitment of both the mTORC2 subunit mSin1 as well as the mTORC2 substrate Akt via their respective PH domains (Ebner *et al.*, 2017a,b).

How might the activation of mTORC2 kinase activity be linked to its kinase-independent roles? Because mTORC2 activity is a mechanosensitive cascade (Berchtold *et al.*, 2012; Diz-Muñoz *et al.*, 2016), it is likely that the same sets of inputs we identify here (Figure 5) could trigger both mTORC2 kinase activity and its scaffolding roles either by recruitment of mTORC2 components (such as PIP_3/PH-domain interaction of mSin1 in mammalian cells; Ebner *et al.*, 2017a) or via local remodeling of mTORC2/Rictor scaffold interactors (such as the release of the TORC2 activator Slm1 from eisosomes in yeast; Berchtold *et al.*, 2012). There is a precedent for this in several other kinase with scaffolding roles including mTORC1 (Erbay and Chen, 2001; Rauch *et al.*, 2011). Similarly, the kinase activity of PI3Kγ and its kinase-independent roles are both triggered downstream from β-adrenergic receptors and work in parallel to regulate cAMP levels (Patrucco *et al.*, 2004; Perino *et al.*, 2011).

A future challenge for the field will be to capture the spatial dynamics of the kinase-dependent and kinase-independent arms of mTORC2. An attractive hypothesis is that the kinase activity of mTORC2 could have a different spatial range to independently regulate myosin-based contractions in regions not constrained by PIP_3. Once mTORC2 kinase activity is triggered, it could induce the phosphorylation of myosin regulators that then diffuse to the trailing edge of the cell. There is a precedent for this in *Dictyostelium* where

activation of Akt/PKB at the leading edge controls a substrate PAKα that acts at the trailing edge (Chung *et al.*, 2001). Future imaging-based activity probes will be necessary to address the spatial logic of mTORC2 activation during cell polarity and movement.

MATERIALS AND METHODS

Cell lines and culture

HL-60 cells were sourced from the laboratory of Henry Bourne and authenticated using short tandem repeat analysis. Cell culture was performed as described previously (Graziano *et al.*, 2019). HL-60 cells were cultured in RPMI-1640 with 25 mM HEPES and l-glutamine (Corning) with 10% (vol/vol) heat-inactivated fetal bovine serum (FBS; Life Technologies) and 1X penicillin/streptomycin (Life Technologies) and maintained at 0.2–1.0 million cells/ml. HL-60 cells were differentiated with 1.5% dimethyl sulfoxide (Sigma-Aldrich) at a starting density of 0.2 million/ml in growth media for 5 d to obtain neutrophil-like dHL-60 cells. All experiments were performed with dHL-60s unless stated otherwise. HEK-293T cells (to generate lentivirus for transducing HL-60s) were cultured in DMEM (Life Technologies) with 10% (vol/vol) heat-inactivated FBS. All cells were cultured in a 37°C/5% CO_2 incubator and routinely monitored for mycoplasma contamination every 6 months.

Plasmids

Plasmids were constructed using standard molecular biology protocols. DNA segments were PCR amplified and cloned into a pHR lentiviral backbone and driven by promoter from spleen focus-forming virus (SFFV) via standard Gibson assembly between the *Mlu*I and *Not*I restriction sites. A construct for Rac biosensor PakPBD-mCherry was generated from PakPBD-mCitrine (Graziano *et al.*, 2019) by switching the DNA encoding the fluorescent tag. The RhoA biosensor uses the AnillinAHPH domain (Piekny and Glotzer, 2008) and was obtained from Addgene (plasmid #68026). The EGFP-AnilinAHPH was subcloned into pHR lentiviral backbone using similar sites and strategy as mentioned above. We modified our previously reported Opto-PI3K module from red-light sensitive Phy/PIF (Graziano *et al.*, 2017) to blue-light sensitive iLID (Guntas *et al.*, 2015). The Opto-PI3K module consists of two constructs that need to be coexpressed for exogenous PIP_3 generation—Construct A: iLiD-BFP-CAAX membrane anchor; Construct B: iSH2-EGFP-SspB scaffold for PI3-kinase recruitment. Both constructs were assembled by Golden Gate–based cloning from a library of individual components from an extendable Mammalian Toolkit (Fonseca *et al.*, 2019) into the pHR vector backbone with EF1α promoter (for Construct A) or SFFV promoter (for Construct B). Guide RNAs (gRNAs) with homology to exon 2 of RICTOR (Rictor KO; 5′ GTCCCGCTGGATCTGACCCG 3′), exon 5 of Rictor (Rictor KO_2; 5′ TAGCACCTTCTGGAGAATAC 3′), exon 2 of MAPKAP1/mSin1 (mSin1 KO; 5′ AGTCAGTCGATATTACCTCA 3′), and exon 5 of MAPKAP1/mSin1 (mSin1 KO_2; 5′ AAACAGTGACTTTAACTCCT 3′) were selected using the CRISPR design tool in Benchling (https://benchling.com/) and cloned into the LentiGuide-Puro vector (Addgene; plasmid #52963) as previously described (Sanjana *et al.*, 2014). The pHR vector used to express human codon–optimized *Streptococcus pyrogenes* Cas9-tag-BFP was as previously described (Graziano *et al.*, 2017).

Lentiviral transduction of HL-60 cells

HEK-293Ts were plated in six-well plates (Corning) and grown to 70–80% confluency. Cells were transfected with 1.5 µg of the pHR plasmid along with two plasmids containing the lentiviral packaging proteins (0.167 µg of pMD2.G and 1.3 µg of p8.91) with TransIT-293 (Mirus Bio). After 2–3 d of transfection, lentivirus-containing supernatant was collected, filtered with a 0.45-µm filter (EMD Millipore), and concentrated 40-fold with Lenti-X Concentrator (Takara). The concentrated lentivirus was used immediately or stored at −80°C. HL-60 cells were transduced by overnight incubation of 0.3 million cells with 4 µg/ml polybrene and ~130 µl of concentrated virus. Cells expressing desired transgenes were isolated by culturing in growth media supplemented with puromycin (1 µg/ml) or using fluorescence-activated cell sorting (FACS) as appropriate (FACS Aria3; BD Biosciences).

Generation of knockout cell lines using CRISPR/Cas9

RICTOR and MAPKAP1(mSin1) HL-60 KO cell lines were generated and validated as previously described (Graziano *et al.*, 2019). WT HL-60 cells were transduced with a puromycin-selectable vector containing the gRNA sequence targeting the gene of interest. Following puromycin selection, cells were transduced with a *S. pyrogenes* Cas9 sequence fused to BFP. Cells expressing high levels of Cas9-BFP were isolated with FACS, after which a heterogeneous population was obtained and assessed by sequencing of the genomic DNA flanking the Cas9 cut site. Cells were then diluted into 96-well plates at a density of approximately one cell per well in 50% (vol/vol) filtered conditioned media from a healthy culture, 40% (vol/vol) fresh HL-60 media, and 10% (vol/vol) additional heat-inactivated FBS. Clonal cell lines were expanded and validated by genomic DNA sequencing to infer the indel distribution and immunoblots to assay loss of protein expression.

Preparation of human neutrophil

All blood specimens were obtained from healthy volunteers with informed consent and using minimal risk protocol approved by the Institutional Review Board at University of California San Francisco (Study 21-35147). Fresh samples of peripheral blood from healthy adult volunteers were collected via 23-gauge butterfly needles in 10 ml BD Vacutainer EDTA tubes (Becton Dickinson, NJ). Blood was kept on a shaker at minimum setting, and utilized within 2 h of the draw. Neutrophils were isolated using the EasySep Direct Human Neutrophil Isolation Kit per the manufacturer's protocol (STEMCELL Technologies).

Cellular treatments and perturbations

Neutrophil-like dHL-60 cells were activated with chemoattractant fMLP (Sigma) at effective final concentration of either 25 nM (for imaging-based assays) or 100 nM (for cellular biochemistry). Acute increase in membrane tension and stretching was done by adding equal volume of hypotonic buffer (H_2O + 1 mM $MgCl_2$ + 1.2 mM $CaCl_2$) as described earlier (Houk *et al.*, 2012; Graziano *et al.*, 2019). mTOR kinase activity was inhibited by treating cells with 10 µM KU-0063794 (Selleckchem) for 30-45 min in plain RPMI-1640. PI3-kinase activity was inhibited by incubating cells with 1 µM PIK-90 for 30–45 min in plain RPMI as described earlier (Van Keymeulen *et al.*, 2006).

Cellular biochemistry

mTORC2 activity (phospho-Akt) assay. These assays were performed as described earlier (Graziano *et al.*, 2017). Cells (dHL-60; 5 d after differentiation) were serum starved to reduce basal pAkt signals by incubation in plain RPMI for 30–45 min at 37°C/5% CO_2 at a density of ~1.5 million cells/ml. All time courses were performed at room temperature (RT) around 25°C. For chemoattractant-based time courses (e.g., Figure 5B), cells were activated at final effective fMLP concentration of 100 nM, and samples were collected at indicated time points by mixing 0.5 ml of

cells with 0.5 ml ice-cold stop solution (20% tricholoroacetic acid [TCA], 40 mM NaF, and 20 mM β-glycerophosphate). Samples were incubated at 4°C for at least 1 hour, after which proteins were pelleted, washed once with 0.75 ml ice-cold 0.5% TCA, and solubilized in 2X Laemmli sample buffer (Bio-Rad Laboratories). For pAkt assays (Supplemental Figure S1C and Figure 5E) cells were assayed in absence (basal level) or 3 min after 100 nM fMLP addition, as pAkt signals peaked at 3 min in our assays. Optogenetic stimulation of Opto-PI3K dHL-60 cells (Figure 5H) was done with the following modifications to the protocol above. Serum-starved cells were placed in wells of a clear-plastic 24-well plate (Corning) and placed about 1 cm above a blue (450 nm) LED array. A ND4 filter (Sioti) was inserted between the cells and the LED light source to attenuate the illumination to 1 mW. Cells were illuminated for 3 min following which the LED was switched off and chilled TCA was added to prepare samples as described above. Samples were then analyzed by immunoblots. Quantification of these assays were done by calculating the ratio of band intensities of phospho-Pak (or Akt) to the total-Pak (or Akt). These values were then normalized to the peak values obtained for WT control in the time series (fMLP 3 min for pAkt).

Immunoblot assay. Western blotting was done as previously described (Graziano *et al*., 2017). Briefly, protein content from at least 0.75-1 million HL-60 cells was extracted by chilled TCA precipitation and resuspended in 2X Laemmli sample buffer. Protein samples were separated via SDS–PAGE, followed by transfer onto nitrocellulose membranes. Membranes were blocked for at least 1 h in a 1:1 solution of TBS (20 mM Tris, 500 mM NaCl, pH 7.4) and Odyssey Blocking Buffer (LI-COR) followed by overnight incubation at 4°C with primary antibodies diluted 1:1000 in a solution of 1:1 TBST (TBS + 0.2% wt/vol Tween 20) and Odyssey Blocking Buffer. Membranes were then washed three times with TBST and incubated for 45 min at RT with secondary antibodies diluted 1:10,000 in 1:1 solution of Odyssey Blocking Buffer and TBST. Membranes were then washed three times with TBST, one time with TBS, and imaged using an Odyssey Fc (LI-COR). Analysis was performed using Image Studio (LI-COR) and Excel. The following primary antibodies were used for the study: phospho-PAK1 (Ser199/204)/PAK2 (Ser192/197) (Cell Signaling; #2605), PAK2 (3B5) (Cell Signaling; #4825), phospho-Akt (Ser473; D9E) XP (Cell Signaling; #4060), Akt (pan; 40D4; Cell Signaling #2920S), Rictor (Bethyl; #A300-458A), mSin1 (Bethyl; #A300-910A), and GAPDH Loading Control Antibody GA1R (Thermo Fisher). Secondary antibodies IRDye 680RD goat anti-mouse (LI-COR) and IRDye 800CW goat anti-rabbit (LI-COR) were used.

Transwell assays

These assays were performed as previously described (Diz-Muñoz *et al*., 2016). Briefly, 0.3 million dHL-60 cells were stained with 5 ul/ml DiD (Life Technologies) and plated on the upper chamber of the 24-well format HTS FluoroBlok Multiwell Insert System (3 μm pore size; BD Falcon) in RPMI without phenol red (Life Technologies) with 2% FBS. Cells were allowed to migrate toward the bottom well containing 20 nM fMLP for 1.5 h at 37°C. The migrated cells were measured by fluorescence from the bottom of the insert using a FlexStation 3 Microplate Reader (Molecular Devices). A migration index was calculated by dividing the amount of signal in the sample well by the signal in a well in which 0.3 million cells were plated in the bottom well. The dataset was normalized by the peak value obtained for WT cells (usually observed at 60 min).

Imaging assays and data analysis

Microscopy hardware. We used a spinning-disk confocal microscope for all imaging data presented here. The setup comprised a Nikon Eclipse Ti inverted microscope with Plan Apo 10×/0.45 NA, 20×/0.75 NA, 60×/1.40 NA, 100×/1.4 NA objectives (Nikon), Yokogawa CSU-X1 spinning-disk confocal, Prime 95B cMOS camera (Photometrics), four-line laser launch (405, 488, 561, and 640 nm laser lines; Vortran), and environmental control (37°C/5% CO_2; Okolab).

Preparation of cells for microscopy. Imaging-based assays with dHL-60 cells were performed using 96-well #1.5 glass-bottom plates (Brooks Life Sciences). The wells were coated with a 100 μl solution of 10 μg/ml porcine fibronectin (prepared from whole blood) and 0.4 mg/ml bovine serum albumin (BSA; endotoxin-free, fatty acid free; A8806; Sigma) dissolved in Dulbecco's phosphate-buffered saline (DPBS; Life Technologies) and incubated for 30 min at RT. Fibronectin solution was then aspirated, and each well was washed twice with DPBS. dHL-60 cells in growth media were pelleted at 300 × *g* for 5 min, resuspended in 100 μl imaging media (RPMI1640 with 0.2% BSA), plated in each well and incubated (37°C/5% CO_2) for 20 min for cells to adhere. Primary human neutrophils were also plated as above and processed similarly as the dHL-60 cells for immunofluorescence assays.

F-actin staining. Cells were prepared and plated in a 96-well glass-bottom plate as described above and stimulated with 25 nM fMLP. After 5 min to allow cells to polarize, an equal volume of 2X fixation buffer (280 mM KCl, 2 mM $MgCl_2$, 4 mM EGTA, 40 mM HEPES, 0.4% BSA, 640 mM sucrose, 7.4% formaldehyde [wt/vol], pH 7.5) was added to each well and incubated for 15 min at RT. The fixation buffer was then removed from each well and cells are washed once with intracellular buffer (140 mM KCl, 1 mM $MgCl_2$, 2 mM EGTA, 20 mM HEPES, 0.2% BSA, pH 7.5). Following fixation, cells were treated with staining buffer (intracellular buffer + 0.2% Triton X-100 + 5 μl/ml Alexa647-phalloidin [Invitrogen]) for 30 min in dark at RT. Cells were finally washed gently to remove excess staining buffer and 200 μl of intracellular buffer mixed with nuclear dye NucBlue (Thermo Fisher) was added to each well.

Immunofluorescence. Cells were prepared, plated, and fixed as above, following which cells were incubated with permeabilization buffer (intracellular buffer and 0.2% Triton X-100) for 20 min at RT. Cells were then blocked (3% BSA and 1% normal goat serum in permeabilization buffer) for at least 1 h at RT. Cells were incubated with primary antibody diluted in blocking solution for at least 2 h at RT or overnight at 4°C. Cells were washed three times with permeabilization buffer and then incubated with secondary antibody for 45 min–1 hour at RT. Finally, cells were washed two times with permeabilization buffer and one time with intracellular buffer before adding fresh intracellular buffer mixed with NucBlue to each well for imaging. Phospho-PAK1 (Ser199/204)/PAK2 (Ser192/197) (Cell Signaling; #2605) and phospho-MLC (Ser19) primary antibody (rabbit; Cell Signaling; #3671) was used at 1:200 dilution with secondary antibody goat anti-rabbit IgG Alexa 488 (Invitrogen; #A-11034) at 1:1000 dilution.

Image analysis for fixed preparations. All image analysis to measure the levels and distribution of F-actin and quantitative immunofluorescence (pPak or pMLC) was performed with Fiji/ImageJ. Briefly, raw images comprising z-stacks of several fields of cells obtained from the Nikon spinning-disk confocal microscope (ND2

format) were imported into Fiji. Before quantification, the images were background and flat-field corrected using the background and flat-field fluorescence values estimated individually for all the different emission channels. Using the z-project tool in Fiji the corrected z-stacks were converted into maximum-intensity projection for visualization and sum-intensity projections for quantification of fluorescence. Intensity thresholds were estimated from the pixel intensity histogram to ignore background fluorescence pixels and uniformly applied to sum-intensity projections to identify cells, following which "measure stack" function was used to measure intensity value for the whole field. Several fields (at least 20–50) with 10–15 cells each were pooled from multiple independent experiments to quantify the fluorescence levels of F-actin, pPak, or pMLC (Figures 2 and 3, and Supplemental Figures S1 and S3) reported here and data was represented as a box-plot to show the entire distribution of measured values. To quantify the width of the F-actin–rich zone at cellular fronts (Figure 2, B and C), a 5-µm-line ROI (2 µm wide) was drawn from the front of the cell to obtain the intensity versus length profile for each cell. Several cells (~20–30 for each condition) were measured and their respective profiles were averaged across the whole dataset. The averaged intensity profile was fitted to a bi-Gaussian distribution (Buys and De Clerk, 1972) of skewed peak to account for the overall width of the F-actin–rich zone. To visualize the 3D distribution of axial z-protrusions of cells, ROIs of individual cell z-stacks were imported into the 3D visualization software UCSF-ChimeraX (Pettersen *et al.*, 2021) and intensity thresholded to highlight the F-actin structures and the cell nuclei. A fraction of cells with axial protrusions was calculated by visual inspection and counting of all cells with 3D projections and the total number of cell nuclei in the entire field of F-actin–stained cells.

Under-agarose preparation of HL-60s for imaging. Cells were prepared using standard under-agarose preparation techniques as described previously (Bell *et al.*, 2018; Brunetti *et al.*, 2022). Briefly, a solution of 2% wt/vol low-melt agarose (Gold Bio) dissolved in RPMI1640 was prepared by heating the solution gently in a microwave. The solution was placed in a water bath at 37°C to cool down before adding to cells. In the meantime, dHL-60 cells were spun down at 300 × *g* for 3 min and resuspended in plating media (RPMI + 2% FBS) at a concentration of 1 million/ml. Cells (5 µl) were placed in the center of a circular well (96-well plate; Greiner Bio-One) and allowed to settle for 5 min at RT. Agarose solution (195 µl) was then slowly dispensed into the well directly on the top of the cells. This allowed even deposition of agarose that congeals over 10–20 min at RT, following which the wells were monitored quickly under a standard tissue culture bright-field microscope and moved to the microscope to equilibrate at 37°C for another 20 min before imaging.

Cell motility assays. Single-cell motility assays were performed with cells plated in an under-agarose preparation (to mimic in vivo–like confined environment) or on fibronectin-coated glass (standard unconfined 2D motility). For both types of motility assays, 0.1 million cells were labeled using 1 µM CellTracker Green or Orange (Thermo Fisher) in plain RPMI for 10 min at 37°C. Labeled cells were spun down from labeling mix and washed once with plain RPMI and resuspended in imaging media (RPMI1640 + 0.5% FBS + NucBlue nuclear marker) and were either plated on fibronectin-coated glass (as described above) or processed for under-agarose preparation and plates were moved to the microscope preheated to 37°C for imaging. Cells were stimulated with a uniform concentration of 25 nm fMLP. To allow tracking of several cell nuclei, imaging was done using a low-magnification objective (10× or 20×) to capture a larger field of view and imaged once every 30 s for more than 20–30 min. Tracking of cell nuclei was performed using the Fiji plug-in TrackMate (Tinevez *et al.*, 2017). Cell nuclei tracks were filtered for the desired property (duration of at least 10 min, high quality, not undergoing collisions) to obtain the coordinates of movement. Track features (like speed, persistence, displacement) were computed with inbuilt tools of TrackMate.

Biosensor imaging. To measure the extent of temporal coordination of front-back polarity, cells expressing both the Rac (PakPBD-mCherry) and RhoA (EGFP-Anilin-AHPH) biosensors were prepared and plated under agarose (2% wt/vol in RPMI1640) and stimulated with uniform chemoattractant (25 nM fMLP). Cells were imaged on a spinning-disk confocal microscope at high spatial resolution (60× or 100× objective) with fast sequential acquisition (exposure time 100 ms) for 3 min at frame intervals of 3 s using a similar strategy as previously described (Tsai *et al.*, 2019). The raw images were background and flat-field corrected, and full images were manually cropped to a ROI with a single cell.

Analysis for spatial distribution of polarity. Spatial profiles of biosensor intensity were obtained from a line ROI (2 µm wide) starting at the leading edge and extending to the uropod to record the intensity versus length traces for both a Rac and a RhoA biosensor. Pearson's correlation coefficients between the two traces were computed for several such individual cells (at least 20–30, pooled from independent experiments) and plotted as box plots. This metric provided an intuitive method to assess the front-back correlation (or lack of it in WT cells) of spatial distribution of polarity signals. To assess the lateral correlation, another line ROI was drawn near the center of the same cells perpendicular to the front-back axis. Intensity profiles for both biosensors were recorded, and lateral correlation coefficients were calculated.

Analysis for temporal coordination of polarity. Cells that touch or collide with a neighboring cell were ignored from this analysis as they presented challenges to segmentation and further analysis. Single cells were then segmented by smoothing and intensity-based thresholding for each of the two emission channels for the biosensor intensities for every frame of the image sequence. The resulting binary images were then combined by taking the union of the two segmentations. Further analysis was done for a sequence of frames where the segmented edge of the cell does not touch the boundary of the cropped image ROI. Using the consensus binary image described above, the weighted centroid of biosensor fluorescence intensity was calculated for each channel across frames. The distances between the coordinates of these centroids were calculated at each frame and the CV of this series was calculated for each cell. The CV provides a normalized metric for fluctuations in the intercentroid distance over the course of the time series and can be readily compared for cells of varying sizes or across different genetic backgrounds (say, WT or Rictor KO cells). The full analysis code is available on GitHub (https://github.com/orgs/weinerlab/repositories).

ACKNOWLEDGMENTS

We thank Jack Strickland for assistance with isolation of primary human neutrophils; Brian Graziano for experimental assistance; Ben Y. Winer and Madhuja Samaddar for critical reading of the manuscript, and members of the Weiner laboratory for stimulating discussions. We thank Kevan Shokat for providing PIK-90. This work was supported by American Heart Association Postdoctoral Fellowship AHA-18POST33990156 (S.S.), UCSF Program for Breakthrough

Biomedical Research Independent Postdoctoral Grant (S.S.), National Science Foundation Graduate Research Fellowship Program (Grant no. 1650113; J.P.T.), National Institutes of Health Grant no. GM-118167 (O.D.W.), National Science Foundation/Biotechnology and Biological Sciences Research Council Grant no. 2019598 (O.D.W.), and the National Science Foundation Center for Cellular Construction (DBI-1548297). We acknowledge the generous support for CVRI microscopy core from UCSF Research Evaluation and Allocation Committee, the Gross Fund, and the Heart Anonymous Fund.

REFERENCES

Agarwal NK, Chen C-H, Cho H, Boulbès DR, Spooner E, Sarbassov DD (2013). Rictor regulates cell migration by suppressing RhoGDI2. Oncogene 32, 2521–2526.

Artemenko Y, Axiotakis L, Borleis J, Iglesias PA, Devreotes PN (2016). Chemical and mechanical stimuli act on common signal transduction and cytoskeletal networks. Proc Natl Acad Sci USA 113, E7500–E7509.

Bell GRR, Natwick DE, Collins SR (2018). Parallel High-Resolution Imaging of Leukocyte Chemotaxis Under Agarose with Rho-Family GTPase Biosensors. New York, NY: Humana Press, 71–85.

Berchtold D, Piccolis M, Chiaruttini N, Riezman I, Riezman H, Roux A, Walther TC, Loewith R (2012). Plasma membrane stress induces relocalization of Slm proteins and activation of TORC2 to promote sphingolipid synthesis. Nat Cell Biol 14, 542–547.

Bercury KK, Dai JX, Sachs HH, Ahrendsen JT, Wood TL, Macklin WB (2014). Conditional ablation of raptor or rictor has differential impact on oligodendrocyte differentiation and CNS myelination. J Neurosci 34, 4466–4480.

Bercury KK, Macklin WB (2015). Dynamics and mechanisms of CNS myelination. Dev Cell 32, 447–458.

Brunetti RM, Kockelkoren G, Raghavan P, Bell GRR, Britain D, Puri N, Collins SR, Leonetti MD, Stamou D, Weiner OD (2022). WASP integrates substrate topology and cell polarity to guide neutrophil migration. J Cell Biol 221, e202104046.

Buys TS, De Clerk K (1972). Bi-Gaussian fitting of skewed peaks. Anal Chem 44, 1273–1275.

Chung CY, Potikyan G, Firtel RA (2001). Control of cell polarity and chemotaxis by Akt/PKB and PI3 kinase through the regulation of PAKa. Mol Cell 7, 937–947.

Diz-Muñoz A, Fletcher DA, Weiner OD (2013). Use the force: membrane tension as an organizer of cell shape and motility. Trends Cell Biol 23, 47–53.

Diz-Muñoz A, Thurley K, Chintamen S, Altschuler SJ, Wu LF, Fletcher DA, Weiner OD (2016). Membrane tension acts through PLD2 and mTORC2 to limit actin network assembly during neutrophil migration. PLoS Biol 14, e1002474.

Ebner M, Lučić I, Leonard TA, Yudushkin I (2017a). PI(3,4,5)P3 engagement restricts Akt activity to cellular membranes. Mol Cell 65, 416–431.e6.

Ebner M, Sinkovics B, Szczygieł M, Ribeiro DW, Yudushkin I (2017b). Localization of mTORC2 activity inside cells. J Cell Biol 216, 343–353.

Eltschinger S, Loewith R (2016). TOR complexes and the maintenance of cellular homeostasis. Trends Cell Biol 26, 148–159.

Erbay E, Chen J (2001). The mammalian target of rapamycin regulates C2C12 myogenesis via a kinase-independent mechanism. J Biol Chem 276, 36079–36082.

Fonseca JP, Bonny AR, Kumar GR, Ng AH, Town J, Wu QC, Aslankoohi E, Chen SY, Dods G, Harrigan P, *et al.* (2019). A toolkit for rapid modular construction of biological circuits in mammalian cells. ACS Synth Biol 8, 2593–2606.

Frias MA, Thoreen CC, Jaffe JD, Schroder W, Sculley T, Carr SA, Sabatini DM (2006). mSin1 is necessary for Akt/PKB phosphorylation, and its isoforms define three distinct mTORC2s. Curr Biol 16, 1865–1870.

Fritz-Laylin LK, Riel-Mehan M, Chen B-C, Lord SJ, Goddard TD, Ferrin TE, Nicholson-Dykstra SM, Higgs H, Johnson GT, Betzig E, Mullins RD (2017). Actin-based protrusions of migrating neutrophils are intrinsically lamellar and facilitate direction changes. eLife 6, 1–41.

García-Martínez JM, Moran J, Clarke RG, Gray A, Cosulich SC, Chresta CM, Alessi DR (2009). Ku-0063794 is a specific inhibitor of the mammalian target of rapamycin (mTOR). Biochem J 421, 29–42.

Gérard A, Patino-Lopez G, Beemiller P, Nambiar R, Ben-Aissa K, Liu Y, Totah FJJ, Tyska MJJ, Shaw S, Krummel MFF (2014). Detection of rare antigen-presenting cells through T cell-intrinsic meandering motility, mediated by Myo1g. Cell 158, 492–505.

Gkountakos A, Pilotto S, Mafficini A, Vicentini C, Simbolo M, Milella M, Tortora G, Scarpa A, Bria E, Corbo V (2018). Unmasking the impact of Rictor in cancer: novel insights of mTORC2 complex. Carcinogenesis 39, 971–980.

Graziano BR, Town JP, Sitarska E, Nagy TL, Fošnarič M, Penič S, Iglič A, Kralj-Iglič V, Gov NS, Diz-Muñoz A, Weiner OD (2019). Cell confinement reveals a branched-actin independent circuit for neutrophil polarity. PLoS Biol 17, e3000457.

Graziano BR, Gong D, Anderson KE, Pipathsouk A, Goldberg AR, Weiner OD (2017). A module for Rac temporal signal integration revealed with optogenetics. J Cell Biol 216, 2515–2531.

Guertin DA, Stevens DM, Thoreen CC, Burds AA, Kalaany NY, Moffat J, Brown M, Fitzgerald KJ, Sabatini DM (2006). Ablation in mice of the mTORC components raptor, rictor, or mLST8 reveals that mTORC2 is required for signaling to Akt-FOXO and PKCα, but not S6K1. Dev Cell 11, 859–871.

Guntas G, Hallett RA, Zimmerman SP, Williams T, Yumerefendi H, Bear JE, Kuhlman B (2015). Engineering an improved light-induced dimer (iLID) for controlling the localization and activity of signaling proteins. Proc Natl Acad Sci USA 112, 112–117.

Hagan GN, Lin Y, Magnuson MA, Avruch J, Czech MP (2008). A Rictor-Myo1c complex participates in dynamic cortical actin events in 3T3-L1 adipocytes. Mol Cell Biol 28, 4215–4226.

Hannigan M, Zhan L, Li Z, Ai Y, Wu D, Huang C-K (2002). Neutrophils lacking phosphoinositide 3-kinase γ show loss of directionality during N-formyl-Met-Leu-Phe-induced chemotaxis. Proc Natl Acad Sci USA 99, 3603–3608.

He Y, Li D, Cook SL, Yoon M-S, Kapoor A, Rao CV, Kenis PJ, Chen J, Wang F (2013). Mammalian target of rapamycin and Rictor control neutrophil chemotaxis by regulating Rac/Cdc42 activity and the actin cytoskeleton. Mol Biol Cell 24, 3369–3380.

Hernández-Negrete I, Carretero-Ortega J, Rosenfeldt H, Hernández-García R, Calderón-Salinas JV, Reyes-Cruz G, Gutkind JS, Vázquez-Prado J (2007). P-Rex1 links mammalian target of rapamycin signaling to Rac activation and cell migration. J Biol Chem 282, 23708–23715.

Hetmanski JHR, de Belly H, Busnelli I, Waring T, Nair RV, Sokleva V, Dobre O, Cameron A, Gauthier N, Lamaze C, *et al.* (2019). Membrane tension orchestrates rear retraction in matrix-directed cell migration. Dev Cell 51, 460–475.e10.

Hind LE, Vincent WJB, Huttenlocher A (2016). Leading from the back: the role of the uropod in neutrophil polarization and migration. Dev Cell 38, 161–169.

Houk AR, Jilkine A, Mejean CO, Boltyanskiy R, Dufresne ER, Angenent SB, Altschuler SJ, Wu LF, Weiner OD (2012). Membrane tension maintains cell polarity by confining signals to the leading edge during neutrophil migration. Cell 148, 175–188.

Huang L, Zhang Y, Xu C, Gu X, Niu L, Wang J, Sun X, Bai X, Xuan X, Li Q, *et al.* (2017). Rictor positively regulates B cell receptor signaling by modulating actin reorganization via ezrin. PLoS Biol 15, e2001750.

Itakura A, Aslan JE, Kusanto BT, Phillips KG, Porter JE, Newton PK, Nan X, Insall RH, Chernoff J, McCarty OJT (2013). p21-Activated kinase (PAK) regulates cytoskeletal reorganization and directional migration in human neutrophils. PLoS One 8, e73063.

Jacinto E, Facchinetti V, Liu D, Soto N, Wei S, Jung SY, Huang Q, Qin J, Su B (2006). SIN1/MIP1 maintains rictor-mTOR complex integrity and regulates Akt phosphorylation and substrate specificity. Cell 127, 125–137.

Jacinto E, Loewith R, Schmidt A, Lin S, Rüegg MA, Hall A, Hall MN (2004). Mammalian TOR complex 2 controls the actin cytoskeleton and is rapamycin insensitive. Nat Cell Biol 6, 1122–1128.

Kamimura Y, Xiong Y, Iglesias PA, Hoeller O, Bolourani P, Devreotes PN (2008). PIP3-independent activation of TorC2 and PKB at the cell's leading edge mediates chemotaxis. Curr Biol 18, 1034–1043.

Katsumi A, Milanini J, Kiosses WB, Del Pozo MA, Kaunas R, Chien S, Hahn KM, Schwartz MA (2002). Effects of cell tension on the small GTPase Rac. J Cell Biol 158, 153–164.

Khanna A, Lotfi P, Chavan AJ, Montaño NM, Bolourani P, Weeks G, Shen Z, Briggs SP, Pots H, Van Haastert PJM, *et al.* (2016). The small GTPases Ras and Rap1 bind to and control TORC2 activity. Sci Rep 6, 25823.

Koronakis V, Hume PJ, Humphreys D, Liu T, Horning O, Jensen ON, McGhie EJ (2011). WAVE regulatory complex activation by cooperating GTPases Arf and Rac1. Proc Natl Acad Sci USA 108, 14449–14454.

Kovalski JR, Bhaduri A, Zehnder AM, Neela PH, Che Y, Wozniak GG, Khavari PA (2019). The functional proximal proteome of oncogenic Ras includes mTORC2. Mol Cell 73, 830–844.e12.

Ku CJ, Wang Y, Weiner OD, Altschuler SJ, Wu LF (2012). Network crosstalk dynamically changes during neutrophil polarization. Cell 149, 1073–1083.
Lai H, Chiou J-G, Zhurikhina A, Zyla TR, Tsygankov D, Lew DJ (2018). Temporal regulation of morphogenetic events in *Saccharomyces cerevisiae*. Mol Biol Cell 29, 2069–2083.
Lämmermann T, Afonso PV, Angermann BR, Wang JM, Kastenmüller W, Parent CA, Germain RN (2013). Neutrophil swarms require LTB4 and integrins at sites of cell death in vivo. Nature 498, 371–375.
Lee S, Comer FI, Sasaki A, McLeod IX, Duong Y, Okumura K, Yates JR, Parent CA, Firtel RA (2005). TOR complex 2 integrates cell movement during chemotaxis and signal relay in *Dictyostelium*. Mol Biol Cell 16, 4572–4583.
Liu L, Das S, Losert W, Parent CA (2010). MTORC2 regulates neutrophil chemotaxis in a cAMP- and RhoA-dependent fashion. Dev Cell 19, 845–857.
Liu L, Gritz D, Parent CA (2014). PKCβII acts downstream of chemoattractant receptors and mTORC2 to regulate cAMP production and myosin II activity in neutrophils. Mol Biol Cell 25, 1446–1457.
Liu Y-J, Le Berre M, Lautenschlaeger F, Maiuri P, Callan-Jones A, Heuzé M, Takaki T, Voituriez R, Piel M (2015). Confinement and low adhesion induce fast amoeboid migration of slow mesenchymal cells. Cell 160, 659–672.
Maiuri P, Rupprecht J-F, Wieser S, Ruprecht V, Bénichou O, Carpi N, Coppey M, De Beco S, Gov N, Heisenberg C-P, *et al.* (2015). Actin flows mediate a universal coupling between cell speed and cell persistence. Cell 161, 374–386.
Morrison Joly M, Williams MM, Hicks DJ, Jones B, Sanchez V, Young CD, Sarbassov DD, Muller WJ, Brantley-Sieders D, Cook RS (2017). Two distinct mTORC2-dependent pathways converge on Rac1 to drive breast cancer metastasis. Breast Cancer Res 19, 74.
Mueller J, Szep G, Nemethova M, de Vries I, Lieber AD, Winkler C, Kruse K, Small JV, Schmeiser C, Keren K, *et al.* (2017). Load adaptation of lamellipodial actin networks. Cell 171, 188–200.e16.
Nawaz S, Sánchez P, Schmitt S, Snaidero N, Mitkovski M, Velte C, Brückner BR, Alexopoulos I, Czopka T, Jung SY, *et al.* (2015). Actin filament turnover drives leading edge growth during myelin sheath formation in the central nervous system. Dev Cell 34, 139–151.
Onwubiko UN, Mlynarczyk PJ, Wei B, Habiyaremye J, Clack A, Abel SM, Das ME (2019). A Cdc42 GEF, Gef1, through endocytosis organizes F-BAR Cdc15 along the actomyosin ring and promotes concentric furrowing. J Cell Sci 132, jcs223776.
Patrucco E, Notte A, Barberis L, Selvetella G, Maffei A, Brancaccio M, Marengo S, Russo G, Azzolino O, Rybalkin SD, *et al.* (2004). PI3Kγ modulates the cardiac response to chronic pressure overload by distinct kinase-dependent and -independent effects. Cell 118, 375–387.
Perino A, Ghigo A, Ferrero E, Morello F, Santulli G, Baillie GS, Damilano F, Dunlop AJ, Pawson C, Walser R, *et al.* (2011). Integrating cardiac PIP3 and cAMP signaling through a PKA anchoring function of p110γ. Mol Cell 42, 84–95.
Pettersen EF, Goddard TD, Huang CC, Meng EC, Couch GS, Croll TI, Morris JH, Ferrin TE (2021). UCSF ChimeraX: Structure visualization for researchers, educators, and developers. Protein Sci 30, 70–82.
Piekny AJ, Glotzer M (2008). Anillin is a scaffold protein that links RhoA, actin, and myosin during cytokinesis. Curr Biol 18, 30–36.
Pipathsouk A, Brunetti RM, Town JP, Graziano BR, Breuer A, Pellett PA, Marchuk K, Tran N-HT, Krummel MF, Stamou D, *et al.* (2021). The WAVE complex associates with sites of saddle membrane curvature. J Cell Biol 220, e202003086.
Rauch J, Volinsky N, Romano D, Kolch W (2011). The secret life of kinases: functions beyond catalysis. Cell Commun Signal 9, 23.
Riggi M, Niewola-Staszkowska K, Chiaruttini N, Colom A, Kusmider B, Mercier V, Soleimanpour S, Stahl M, Matile S, Roux A, Loewith R (2018). Decrease in plasma membrane tension triggers PtdIns(4,5)P_2 phase separation to inactivate TORC2. Nat Cell Biol 20, 1043–1051.
Riggi M, Kusmider B, Loewith R (2020). The flipside of the TOR coin – TORC2 and plasma membrane homeostasis at a glance. J Cell Sci 133, jcs242040.
Saci A, Cantley LC, Carpenter CL (2011). Rac1 regulates the activity of mTORC1 and mTORC2 and controls cellular size. Mol Cell 42, 50–61.
Saha S, Nagy TL, Weiner OD (2018). Joining forces: crosstalk between biochemical signalling and physical forces orchestrates cellular polarity and dynamics. Philos Trans R Soc B Biol Sci 373, 20170145.
Sanjana NE, Shalem O, Zhang F (2014). Improved vectors and genome-wide libraries for CRISPR screening. Nat Methods 11, 783–784.
Sarbassov DD, Ali SM, Kim D-H, Guertin DA, Latek RR, Erdjument-Bromage H, Tempst P, Sabatini DM (2004). Rictor, a novel binding partner of mTOR, defines a rapamycin-insensitive and raptor-independent pathway that regulates the cytoskeleton. Curr Biol 14, 1296–1302.
Saxton RA, Sabatini DM (2017). mTOR signaling in growth, metabolism, and disease. Cell 169, 361–371.
SenGupta S, Parent CA, Bear JE (2021). The principles of directed cell migration. Nat Rev Mol Cell Biol 22, 529–547.
Senoo H, Kamimura Y, Kimura R, Nakajima A, Sawai S, Sesaki H, Iijima M (2019). Phosphorylated Rho–GDP directly activates mTORC2 kinase towards AKT through dimerization with Ras–GTP to regulate cell migration. Nat Cell Biol 21, 867–878.
Srinivasan S, Wang F, Glavas S, Ott A, Hofmann F, Aktories K, Kalman D, Bourne HR (2003). Rac and Cdc42 play distinct roles in regulating PI(3,4,5)P_3 and polarity during neutrophil chemotaxis. J Cell Biol 160, 375–385.
Stephens L, Smrcka A, Cooke FT, Jackson TR, Sternweis PC, Hawkins PT (1994). A novel phosphoinositide 3 kinase activity in myeloid-derived cells is activated by G protein βγ subunits. Cell 77, 83–93.
Tinevez J-Y, Perry N, Schindelin J, Hoopes GM, Reynolds GD, Laplantine E, Bednarek SY, Shorte SL, Eliceiri KW (2017). TrackMate: an open and extensible platform for single-particle tracking. Methods 115, 80–90.
Tsai TY-C, Collins SR, Chan CK, Hadjitheodorou A, Lam P-Y, Lou SS, Yang HW, Jorgensen J, Ellett F, Irimia D, *et al.* (2019). Efficient front-rear coupling in neutrophil chemotaxis by dynamic myosin II localization. Dev Cell 49, 189–205.e6.
Van Keymeulen A, Wong K, Knight ZA, Govaerts C, Hahn KM, Shokat KM, Bourne HR (2006). To stabilize neutrophil polarity, PIP3 and Cdc42 augment RhoA activity at the back as well as signals at the front. J Cell Biol 174, 437–445.
Wang F, Herzmark P, Weiner OD, Srinivasan S, Servant G, Bourne HR (2002). Lipid products of PI(3)Ks maintain persistent cell polarity and directed motility in neutrophils. Nat Cell Biol 4, 513–518.
Weiner OD, Marganski WA, Wu LF, Altschuler SJ, Kirschner MW (2007). An actin-based wave generator organizes cell motility. PLoS Biol 5, 2053–2063.
Weiner OD, Neilsen PO, Prestwich GD, Kirschner MW, Cantley LC, Bourne HR (2002). A PtdInsP3- and Rho GTPase-mediated positive feedback loop regulates neutrophil polarity. Nat Cell Biol 4, 509–513.
Wong K, Pertz O, Hahn K, Bourne H (2006). Neutrophil polarization: spatiotemporal dynamics of RhoA activity support a self-organizing mechanism. Proc Natl Acad Sci USA 103, 3639–3644.
Xu J, Wang F, Van Keymeulen A, Herzmark P, Straight A, Kelly K, Takuwa Y, Sugimoto N, Mitchison T, Bourne HR (2003). Divergent signals and cytoskeletal assemblies regulate self-organizing polarity in neutrophils. Cell 114, 201–214.
Yang Q, Zhang X-F, Van Goor D, Dunn AP, Hyland C, Medeiros N, Forscher P (2013). Protein kinase C activation decreases peripheral actin network density and increases central nonmuscle myosin II contractility in neuronal growth cones. Mol Biol Cell 24, 3097–3114.